ENGINEERING RESEARCH INSTITUTE
THE UNIVERSITY OF MICHIGAN
ANN ARBOR

Status Report

THEORETICAL AND EXPERIMENTAL STUDIES OF THE REFLECTION OF SOUND FROM ROUGH SURFACES AND THE PROPAGATION OF SOUND IN SHALLOW WATER

Julian R. Frederick
William C. Meecham
Irene V. Schensted
James E. Lesch

Project 1936

OFFICE OF NAVAL RESEARCH, U.S. NAVY DEPARTMENT
CONTRACT N6 onr 23221, PROJECT NR 385-203

April 1956

Engm
UMR
1499

TABLE OF CONTENTS

TABLE OF CONTENTS (Continued)

LIST OF TABLES

LIST OF FIGURES

LIST OF FIGURES (Continued)

LIST OF FIGURES (Concluded)

I. INTRODUCTION

The purpose of this report is to review the research effort as it has progressed in the period from 1 August 1954 to 31 December 1955 on contract N6 onr 23221, Project NR 385-203. During this period a significant change has occurred in the type of research employed on this project in the study of underwater sound propagation.

Heretofore the main emphasis had been placed upon statistical and theoretical analyses of certain types of underwater sound propagation data and submarine contact data as collected by various naval and Navy-sponsored activities. The analyses were made to investigate the role of certain factors in the environment on underwater sound propagation and target detection.

As will be evident in this report there have been two major divisions of the research conducted over the past year. The work has followed closely the outline submitted in a contract renewal proposal dated in November of 1954. The two major divisions are listed below.

a. Theoretical studies of the scattering of radiation by rough surfaces.

b. Theoretical and experimental model studies of the propagation of sound in shallow water.

The theoretical work devoted to the rough surface effects is briefly reviewed in section 2.0 of this report. A separation of this from the theoretical approach to shallow water model studies is made for the reason that the rough surface material is not directly related to the model study. In addition, the rough surface work has in large part been accepted for publication

in various scientific journals. No experimental effort has been expended during this period on rough surface scattering effects by this project.

In section 3.0 of this report both the theoretical and experimental phases of the model program are reviewed. For the most part the model program has dealt with situations where the water depth is equal to a few radiation wave lengths. Underwater sound propagation has been studied over the concrete tank bottom using both continuous-wave and pulsed signals. Acoustical constants of the bottom and the effects of changing frequency and water depth have been examined.

More specifically section 3.1 contains the theoretical treatment of the following subjects --

a. acoustic pressure as a function of range (normal mode approach) for a harmonic source and three different bottom types,
b. effect of an extended source on the field pattern,
c. prediction of pulse shape as a function of range for short pulses,
d. comparison of an image theory versus normal mode theory for prediction of pulse shape,
e. bottom reflection coefficients for specific conditions.

Section 3.2 contains a description of the model experiments and a discussion of the results obtained. The experiments were designed primarily to explore the characteristics of the model for water depths of the order of magnitude of the wave length. The section is broken into subsections treating the following subjects --

a. equipment and techniques,

b. continuous-wave experiments,

c. pulse experiments,

d. bottom characteristics,

e. summary and conclusions.

II. A THEORETICAL INVESTIGATION OF THE REFLECTION OF RADIATION FROM PERIODIC AND IRREGULAR SURFACES

W.C. Meecham

The results of work on this class of problems may be collected under three main subject heads. The major part of the effort expended during the period of time covered by this report has been devoted to the consideration of the variational method (see below). These three topics are covered in detail in separate reports under the titles given. Only brief summaries of these reports are given here.

2.1. ON THE USE OF THE KIRCHHOFF APPROXIMATION FOR THE SOLUTION OF REFLECTION PROBLEMS

The methods of physical optics can be applied to reflection problems under certain circumstances. As is well known these methods are based upon the Kirchhoff approximation, which is an assumption concerning the value of the radiation field near the reflecting surface. It is assumed in the approximation that the field near every region of the surface is essentially what it would have been if the surface had been flat with a slope equal to that of the irregular surface at the point in question. Using this assumption concerning the value of the field at the bounding surface in conjunction with the Helmholtz formula it is possible to obtain an estimate of the field in regions removed from the reflecting surface. It is shown that this assumption is valid if the following two restrictions hold:

i) $\left|\frac{d\zeta^M}{dx}\right| \ll 1$

ii) $kR_m \gg 1$,

where $\left(\frac{d\zeta}{dx}\right)_M$ is the maximum value of the slope of the reflecting surface, $k = 2\pi/\lambda$ where λ is the radiation wave length, and R_m is the minimum radius of curvature of the reflecting surface. Furthermore it is shown that the results obtained by the use of the Kirchhoff approximation satisfy the reciprocity theorem.

2.2. A FOURIER TRANSFORM METHOD FOR THE TREATMENT OF THE PROBLEM OF THE REFLECTION OF RADIATION FROM IRREGULAR SURFACES

A method is presented which can be used for the calculation of the distribution of energy reflected from irregular surfaces. The formulation is useful for the first boundary value problem and can be used in either two- or three-dimensional problems with any given incident field. The solution is reduced to quadrature with negligible error when the average square of the slope of the reflecting surface is small and when the wave length of the incident radiation is not small compared with the displacement of the surface from its average value. A numerical example is worked, the sinusoidal surface, and is compared with experiment and with a method due to Rayleigh. It is found that the Fourier transform method is preferable to previous methods, notably those which can be classified as physical optics (such as Rayleigh's) since the error in the transform method is of second order in the surface slope whereas the error in previous methods is of first order in the same quantity.

2.3. A VARIATIONAL METHOD FOR THE CALCULATION OF THE DISTRIBUTION OF ENERGY REFLECTED FROM A PERIODIC SURFACE

A variational method is presented which is used to calculate the energy appearing in the various diffracted orders set up when a plane wave is incident upon a periodic reflecting surface. Either the first or the second boundary condition can be so treated. A sample problem is worked showing

that if the average absolute slope of the reflecting surface is small (segments of surface with large slope may be included) and if the displacement of the surface is not large compared with the wave length of the incident radiation, the formulation gives results correct to within a few per cent. The calculation shows clearly the existence of Wood anomalies; these are discussed in some detail.

III. AN INVESTIGATION OF THE PROPAGATION OF SOUND FROM A POINT SOURCE IN A LIQUID LAYER OVER CONCRETE

3.0. MODEL PROGRAM

For the purpose of gaining a better understanding of the mechanism of sound propagation in shallow water an acoustic model program has been initiated. By this means it is desired to secure a borader knowledge of the fundamentals of some of the simpler shallow water problems. If this can be done both by experiment and by theory the plan is to turn to progressively more complex situations. It is hoped that the model may serve as an analogue computer in the investigation of phenomena too complex for adequate theoretical treatment.

This section of the report describes experimental and theoretical approaches to some of the less complex problems. It contains descriptions of the use of a concrete tank model in experiments and examples of the application of normal mode theory to these problems.

Shallow water is defined for the purposes of this report as the depth at which sound propagation is best treated theoretically by normal mode theory (as opposed to a ray treatment). The effort has been confined to the study of propagation in situations where the water depth is approximately twice the radiation wave length. The ranges vary from a few up to 40 or 50 wave lengths.

3.1. THEORETICAL CONSIDERATIONS

Irene Schensted

During the course of the investigation various calculations have been made in connection with the study of the propagation of sound in a fluid layer over a concrete bottom. It is the purpose of this part of the report to present the results of these calculations. Specifically, they have been carried out to determine the acoustical pressure as a function of range for a time harmonic source using three models to represent the behavior of the bottom: (1) a fluid (water) layer over a rigid bottom, (2) a fluid layer over a semi-infinite fluid capable of transmitting compressional waves, and (3) a fluid layer over a semi-infinite solid capable of transmitting both shear and compressional waves. Comparison was made of the predictions of these three models with the experimental results with a view to determining the simplest model which might suffice to predict the results of the pertinent experiments. Although the concrete bottom of the tank was finite in extent, a series of simple calculations such as those performed in the appendix of this report indicate that the assumption of an infinite bottom is a good approximation to the actual case.

The calculations are based on the normal mode theory of sound propagation. The basic work in this field is given by a classical paper by Lamb.[1] In section 3.1.1 below are presented the results of the normal mode theory for the three models cited above. The formulas used are taken from Pekeris[2] and Press and Ewing.[3] The reader is referred to the work of the authors of these two references for derivations of these formulas.

Calculations are also made to determine the pulse shapes to be expected as function of range for short pulses. In this study it is found convenient to use the method of images to supplement the normal mode point of view. Section 3.1.2 deals with the problem of the pulse shape to be expected

under various conditions and exhibits the results of the pulse shape calculations.

3.1.1. Calculations Based on the Normal Mode Representation of the Solution

In this section are presented calculations based on the normal mode representation of the solution for the following types of bottom: (1) rigid, (2) semi-infinite fluid, and (3) a semi-infinite elastic.

The Rigid Bottom - We shall assume a point source to be located at a depth d from the upper surface of a liquid layer of depth H. We shall use a cylindrical coordinate system with coordinates r, θ, and z, with an origin on the surface of the liquid vertically above the source. The positive z axis passes through the source and is oriented normal to the top and bottom surfaces as shown in Fig. 1.

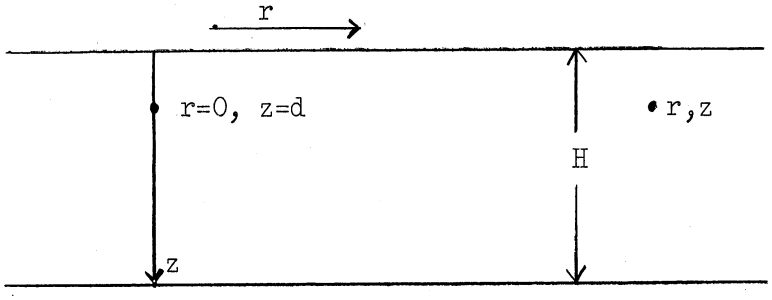

Fig. 1. The Geometry of the Model

The surface $z = 0$ is to be thought of as a free surface (a surface of zero excess acoustic pressure). The bottom at $z = H$ is for the present to be thought of as being perfectly rigid so that the z component of the velocity of the fluid at that plane is zero.

All quantities of physical interest in this problem may be derived from a scalar potential function ψ which satisfies the wave equation

$$\nabla^2\psi - \frac{1}{c^2}\frac{\partial^2\psi}{\partial t^2} = 0$$

where c is the phase velocity of acoustic waves in the liquid. In addition it is necessary that ψ satisfy certain boundary conditions. The

velocity $\vec{v}$ of any point in the liquid layer is related to ψ by the relationship $\vec{v} = -\nabla\psi$. The excess acoustical pressure p is related to by the relationship $p = \rho \frac{\partial \psi}{\partial t}$ where ρ is the density of the liquid. Hence since $v_z = 0$ at $z = H$ and since $p = 0$ at $z = 0$, the scalar potential ψ must satisfy the following boundary conditions:

$$\psi = 0 \quad \text{at} \quad z = 0 ,$$

and

$$\frac{\partial \psi}{\partial z} = 0 \quad , \quad z = H .$$

In addition ψ must behave like a point source in the vicinity of $r = 0$, $z = d$. For a time harmonic point source of frequency $\frac{\omega}{2\pi}$, this means that

$$\psi(r,z,t) \longrightarrow \frac{e^{i\omega(t-\sqrt{r^2 + (z-d)^2}/c)}}{\sqrt{r^2 + (z-d)^2}}$$

as $r \to 0$ and $z \to d$.

In this section only a time harmonic point source of time dependence $e^{i\omega t}$ will be considered. If one finds the response, $R(\omega,r,z)$, of the medium to such a time harmonic excitation, then the response to the more general excitation $f(t)$ will simply be

$$\frac{1}{\sqrt{2\pi}} \int_{-\infty}^{\infty} R(\omega,r,z)g(\omega)e^{i\omega t}d\omega$$

where $g(\omega)$ is the Fourier transform of $f(t)$ defined by

$$g(\omega) = \frac{1}{\sqrt{2\pi}} \int_{-\infty}^{\infty} f(t)e^{-i\omega t}dt .$$

In section 3.1.2 the response to finite time pulses will be discussed. Accordingly for the present, set $\psi = \phi(r,z)e^{i\omega t}$ where $\phi(r,z)$ must satisfy the equation $\nabla^2\phi = -k_0^2\phi$, with $k_0 = \omega/c = 2\pi/\lambda_0$; λ_0 is the

radiation wave length in the fluid layer. Also ϕ must satisfy the boundary conditions

$$\phi = 0 \quad \text{at} \quad z = 0 \ ,$$

and

$$\frac{\partial \phi}{\partial z} = 0 \quad \text{at} \quad z = H \ ,$$

as well as the condition that it behave like a point source near $r = 0$, $z = d$.

The solution to the problem stated above may be expressed in the following integral form:

$$\psi = \begin{cases} e^{i\omega t} \int_0^\infty J_0(kr) \, \frac{2k}{\beta} \sin \beta z \cos \beta(d-H) \, dk \ , & 0 \leq z \leq d \ ; \\ e^{i\omega t} \int_0^\infty J_0(kr) \, \frac{2k}{\beta} \, \frac{\sin \beta d \cos \beta(z-H)}{\cos \beta H} \, dk \ , & d \leq z \leq H \ ; \end{cases} \tag{1}$$

where $\beta = \sqrt{k_0^2 - k^2}$ $\qquad k_0 \geq k \ ,$

and $\beta = -i \sqrt{k^2 - k_0^2}$ $\qquad k \geq k_0 \ ,$

and $J_0(x)$ is the Bessel function of the first kind. The path of integration in Eq. (1) makes semi-circular detours about those poles of the integrand which lie on the real axis as shown in Fig. 2.

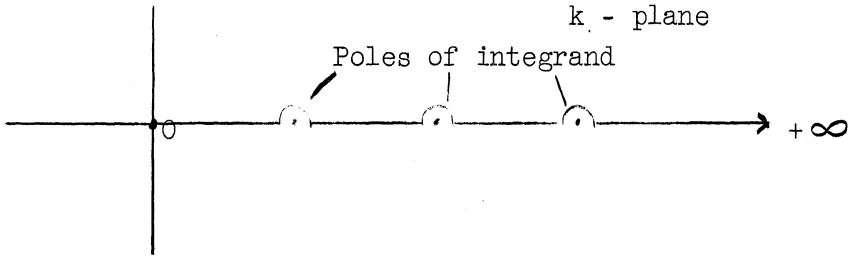

Fig. 2. Path of Integration for the integral, representation of the solution of the propagation problem.

The integrands in the above expression are, for k arbitrary, solutions of the wave equation which satisfy the given boundary conditions at $z = 0$ and $z = H$. These solutions are integrated over the path indicated in k space with the given weighting factors so as to yield the desired point source behavior at $r = 0$, $z = d$. This technique of integrating kernels, which satisfy the wave equation and appropriate boundary conditions, so as to yield point source behavior is used frequently in problems of this type.

The above integral representation may be transformed to a sum of residues by the use of Cauchy's integral theorem. The resulting expression is:

$$\psi = e^{i\omega t}\,\frac{(-2\pi i)}{H}\sum_{n=0}^{\infty} H_0^{(2)}(k_n r)\sin\left[(n+\tfrac{1}{2})\frac{\pi d}{H}\right]\sin\left[(n+\tfrac{1}{2})\,\frac{\pi z}{H}\right] \qquad (2)$$

$$0 \leq z \leq H\ ,$$

where $k_n = \sqrt{\omega^2/c^2 - (n+\frac{1}{2})^2\,(\pi/H)^2}$ $\qquad (n+\frac{1}{2})\,\pi/H < \omega/c$

$$k_n = -i\sqrt{((n+\tfrac{1}{2})\,\pi/H)^2 - \omega^2/c^2} \qquad \omega/c < (n+\tfrac{1}{2})\,\pi/H$$

$H_0^{(2)}$ is the zeroth order Hankel function of the second kind. The above representation is usually called the normal mode form of the solution, each term being called a mode. Asymptotically for large r,

$$H_0^{(2)}(k_n r) \to \sqrt{\frac{2}{\pi k_n r}}\, e^{-ik_n r + i\pi/4} \qquad |k_n| r >> 1\ .$$

Hence for large r the normal mode form is:

$$\psi \simeq -2\pi i e^{i\omega t}\sum_{n=0}^{\infty}\sqrt{\frac{2}{\pi k_n r}}\, e^{-ik_n r + i\pi/4}\,\frac{\sin\left[(n+\frac{1}{2})\pi d/H\right]\sin\left[(n+\frac{1}{2})\pi z/H\right]}{H}$$

$$0 \leq z \leq H\ .$$

For n sufficiently great it is apparent that k_n will be imaginary and the corresponding modes will not propagate. The largest integer n_{max} which satisfies the equation $(n+\frac{1}{2})\,\pi < H\,\omega/c$ will determine the number of modes

propagating in the medium; the cut-off frequency for the n^{th} mode will be $\frac{\omega}{2\pi} = (n+\frac{1}{2})\frac{c}{2H}$.

In Fig. 3* the amplitude of the acoustical pressure is plotted versus range for the following special case:

$$\omega/2\pi = 4800/\text{sec.}$$

$$c = 4800 \text{ ft/sec.}$$

$$H = 2\lambda_0$$

$$z = d = H/2 \text{ .}$$

These parameters were chosen so as to correspond to the conditions under which some of the experiments were performed in the model tank. For this case there are only four propagating modes corresponding to $n = 0$, $n = 1$, $n = 2$, $n = 3$. The fifth mode corresponding to $n = 4$ yields a value of $k_4 = -\sqrt{\frac{17}{16}}\,\pi i$. Hence at a range of 10 feet the amplitude of this mode compared to that of any one of the undamped four would be of the order of $e^{-10.3\pi} \sim 10^{-14}$. The succeeding terms in the series are even smaller. It may be shown that

$$\sum_{n=4}^{\infty} e^{-10\sqrt{(n+\frac{1}{2})^2 \pi 2/4 - (4\pi)^2}} < e^{-10.3\pi}\left(\frac{1}{1 - e^{-10.3\pi}}\right) \simeq e^{-10.3\pi}$$

In view of this fact one need only consider the first four modes in calculating the pattern of the acoustical pressure for these conditions. The normal mode series therefore constitutes a very practical approach to the problem of getting numerical results for large ranges for continuous-wave sources because of the series' rapid convergence. We shall see in section 3.1.2 that the image series representation of the solution of this problem is not rapidly convergent for large ranges.

---

* The acoustic pressure units are arbitrary; in the present study only relative values were of interest.

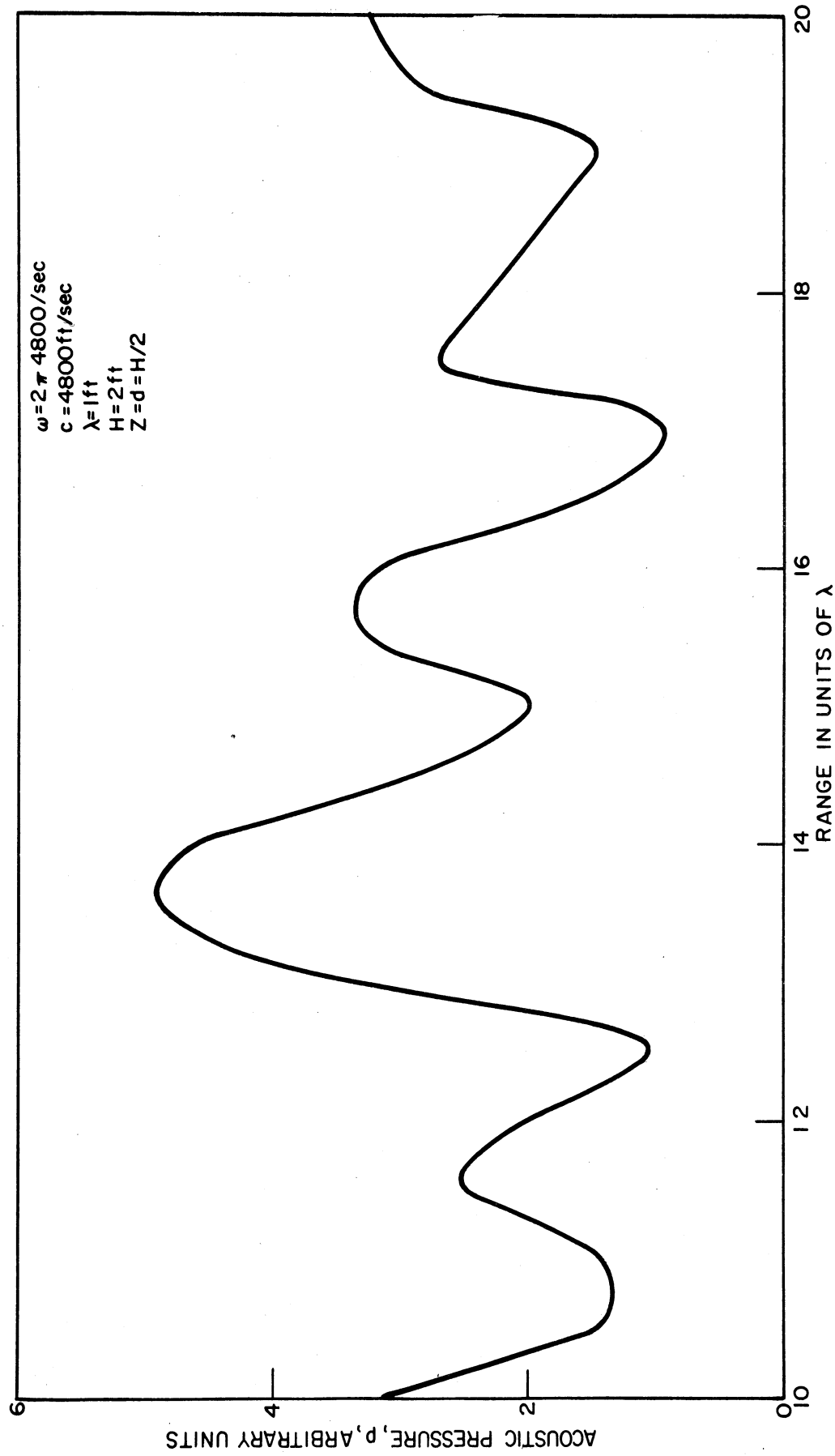

Fig. 4. Calculated acoustic pressure variation with range for the rigid bottom model employing an extended source. Source length is 0.2λ.

Before going on to consider the two fluid cases note that source and receiver depth appear only in the form of the factor $\sin(n+\frac{1}{2})\frac{\pi z}{H}\sin(n+\frac{1}{2})\frac{\pi d}{H}$. For a linearly extended source one may therefore take into account source extension by integrating the factor $\sin(n+\frac{1}{2})\frac{\pi d}{H}$ with respect to a weighing function representing source strength along the source line. Since the source used in the experiment was not exactly a point source it is of interest to carry out calculations taking into account this effect. For a uniform linear source of length ℓ and of unit total strength one would obtain the solution ($kr \gg 1$):

$$\psi \cong -\frac{2\pi i}{H} e^{i\omega t} \sum_{n=0}^{\infty} \frac{e^{-ik_n r + i\pi/4}}{\sqrt{\frac{\pi}{2} k_n r}} \frac{\cos \beta_n(d-\frac{\ell}{2}) - \cos \beta_n(d+\frac{\ell}{2}) \sin \beta_n z}{\beta_n \ell} \qquad (3)$$

One may account for receiver extension in a similar way. Figure 4 exhibits the effect of source extension on the pattern. The ω and H are assumed to be the same as for the case mentioned above but the source is considered to be uniformly linearly extended, of 25 inches length.

The main effect here is seen to be a change in the relative amplitudes of the peaks and valleys.

The Two Fluid Model - Suppose now that the bottom is capable of transmitting compressional waves. The details of the solution are to be found in a paper by Pekeris.[2] Here it will suffice to describe the nature of the results and the calculations based on them.

Let ρ_2 designate the density of the bottom and c_2 the phase velocity of sound in the bottom. The geometry of the situation is as depicted in Fig. 5.

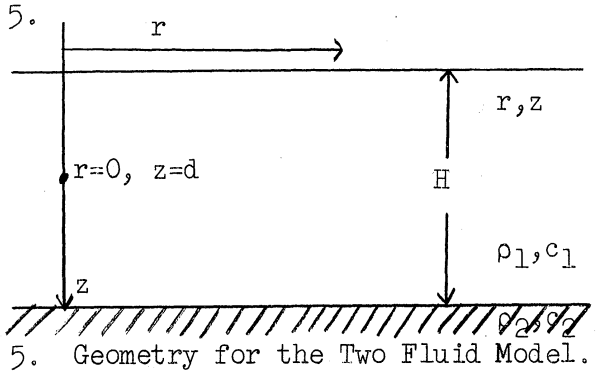

Fig. 5. Geometry for the Two Fluid Model.

The conditions to be satisfied by the excess acoustic pressure are as follows:

$$\nabla^2\psi = \frac{1}{c_1^2}\frac{\partial^2\psi}{\partial t^2} \qquad 0 < z < H$$

$$\nabla^2\psi = \frac{1}{c_2^2}\frac{\partial^2\psi}{\partial t^2} \qquad z > H ,$$

and $\psi = 0$ at $z = 0$ (acoustical pressure is 0 at surface of liquid). At $z = H$ we must require that the acoustical pressure be continuous across the interface separating the two media, and also that v_z be continuous.

$$\rho_1 \frac{\partial\psi}{\partial t}_{z \to H_-} = \rho_2 \frac{\partial\psi}{\partial t}_{z \to H_+} \quad ; \qquad \frac{\partial\psi}{\partial z}_{z \to H_-} = \frac{\partial\psi}{\partial z}_{z \to H_+}$$

where the symbol $z \to H_-$ denotes z approaches H from the domain $z < H$, and the symbol $z \to H_+$ denotes z approaches H from the domain $z > H$.

In addition we have the requirement that ψ behave like a point source in the vicinity of $r = 0$, $z = d$ (see section 3.1.1).

The solution to the time harmonic problem which satisfies the above conditions has the following integral representation:

$$\psi = 2e^{i\omega t}\int_0^\infty J_0(kr)\,\frac{k \sin\beta_1 z}{\beta_1}\left[\frac{\beta_1\cos\beta_1(H-d) + ib\beta_2\sin\beta_1(H-d)}{\beta_1\cos\beta_1 H + ib\,\beta_2\sin\beta_1 H}\right] dk \qquad \text{for } 0 \leq z \leq d$$

$$\psi = 2e^{i\omega t}\int_0^\infty J_0(kr)\,\frac{k \sin\beta_1 d}{\beta_1}\left[\frac{\beta_1\cos\beta_1(H-z) + ib\beta_2\beta_1\,(H-z)}{\beta_1\cos\beta_1 H + ib\,\beta_2\sin\beta_1 H}\right] dk \qquad \text{for } d \leq z \leq H ,$$

and

$$\psi = 2e^{i\omega t_b}\int_0^\infty \frac{J_0(kr)k(\sin\beta_1 d)\,e^{-i\beta_2(z-H)}}{\beta_1\cos\beta_1 H + ib\,\beta_2\sin\beta_1 H}\,dk \qquad z > H , \qquad (4)$$

where
$$\beta_1 = \sqrt{\omega^2/c_1^2 - k^2} \qquad k < \omega/c_1,$$
$$= -i\sqrt{k^2 - \omega^2/c_1^2} \qquad k > \omega/c_1;$$
$$\beta_2 = \sqrt{\omega^2/c_2^2 - k^2} \qquad k < \omega/c_2,$$
$$= -i\sqrt{k^2 - \omega^2/c_2^2} \qquad k > \omega/c_2 .$$

The integrands in the above integral formulas satisfy the wave equation and the boundary conditions at $z = 0$ and $z = H$. The integration over the real axis in the k plane serves to give the desired point source behavior at $r = 0$, $z = d$. The path of integration over the k axis makes semi-circular detours about the poled which occur on the real axis as was shown in Fig. 2.

To obtain the normal mode form of the solution one must transform these integrals to a sum of residues of poles in the complex k plane. The integrands of the integrals in Eq. (4) are not single-valued; they have a branch point at $k = \omega/c_2$. Hence one obtains upon transformation, in addition to the normal mode series, a branch line integral extending along both sides of a branch cut extending from $k = \omega/c_2$ to $k = \omega/c_2 - i\infty$ as shown in Fig. 6.

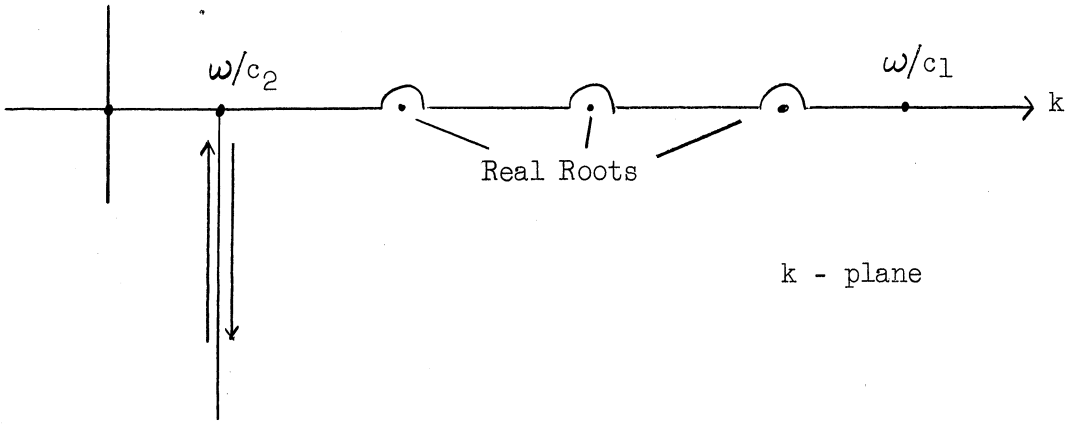

Fig. 6. Position of the poles and the branch line for the integrands of the integral representation of the solution when $c_2 > c_1$.

The following is the normal mode form of the solution which is valid in the top layer ($0 \leq z \leq H$),

$$\psi = e^{i\omega t}\left\{\frac{-2\pi i}{H}\sum_{n=0}^{\infty}\frac{H_0^{(2)}(k_n r)\beta_{1n}H(\sin\beta_{1n}d)\sin\beta_{1n}z}{\left[\beta_{1n}H-(\sin\beta_{1n}H)\cos\beta_{1n}H-b^2(\sin^2\beta_{1n}H)\tan\beta_{1n}H\right]}\right.$$

$$\left. - 2ib\int_{k_2-i\infty}^{k_2}\frac{H_0^{(2)}(kr)\,k\,\beta_2(\sin\beta_1 d)\sin\beta_1 z}{\left[\beta_1^2\cos^2\beta_1 H + b^2\beta_2^2\sin^2\beta_1 H\right]}\,dk\right\} \qquad (5)$$

$0 \leq z \leq H$

with $b = \rho_1/\rho_2$. In Eq. (5) the β_{1n} are the roots of the following transcendential equation (called the period equation),

$$\tan \beta_1 H = - \frac{\beta_1}{b\left(\omega^2/c_1^2 - \omega^2/c_2^2 - \beta_1^2\right)^{1/2}} \qquad (6)$$

The k_n are related to the β_{1n} by the relation: $k_n^2 = \omega^2/c_1^2 - \beta_{1n}^2$.

Before going on to a further discussion of the roots of Eq. (6) we shall present the asymptotic form of the normal mode solution valid for large r. We have

$$\psi \sim e^{i\omega t}\left\{\frac{-2\pi i}{H}\sum_{n=0}^{\infty}\frac{e^{-ik_n r + i\pi/4}}{\sqrt{\frac{\pi k_n r}{2}}}\frac{\beta_{1n}H(\sin\beta_{1n}d)\sin\beta_{1n}z}{\left[\beta_{1n}H-(\sin\beta_{1n}H)\cos\beta_{1n}H-\frac{\sin^3\beta_{1n}H}{\cos\beta_{1n}H}\frac{a}{b}\right]}\right.$$

$$\left. - \frac{2ib\, e^{-ik_2 r}\, k_2 \sin(kr_1\mu d)\sin(k_1\mu z)}{(k_1 r)^2\mu^2\cos^2(\mu H k_1)}\right\},$$

where $\mu = \sqrt{1 - c_1^2/c_2^2}$, $c_1 < c_2$.

The above form is valid providing the parameters are such that $\cos^2(\mu H k_1)$ is not near zero. It is seen from this expression that since the individual propagating modes decrease as $r^{1/2}$ and the branch line contribution decreases as r^2 , that for r sufficiently large, one need only consider the normal mode terms.

To proceed, if we make the substitution $x = \beta_1 H$ in Eq. (6) the period equation may be written as:

$$\tan x = - \frac{x}{b\,H\left(\omega^2/c_1^2 - \omega^2/c_2^2 - \frac{x^2}{H^2}\right)^{1/2}} .$$

There are only a finite number of real roots to this equation. These real roots correspond to the undamped or propagating modes. The real roots can occur only when $c_2 > c_1$ and in the interval $\omega/c_2 \leq k \leq \omega/c_1$. For $c_2 < c_1$

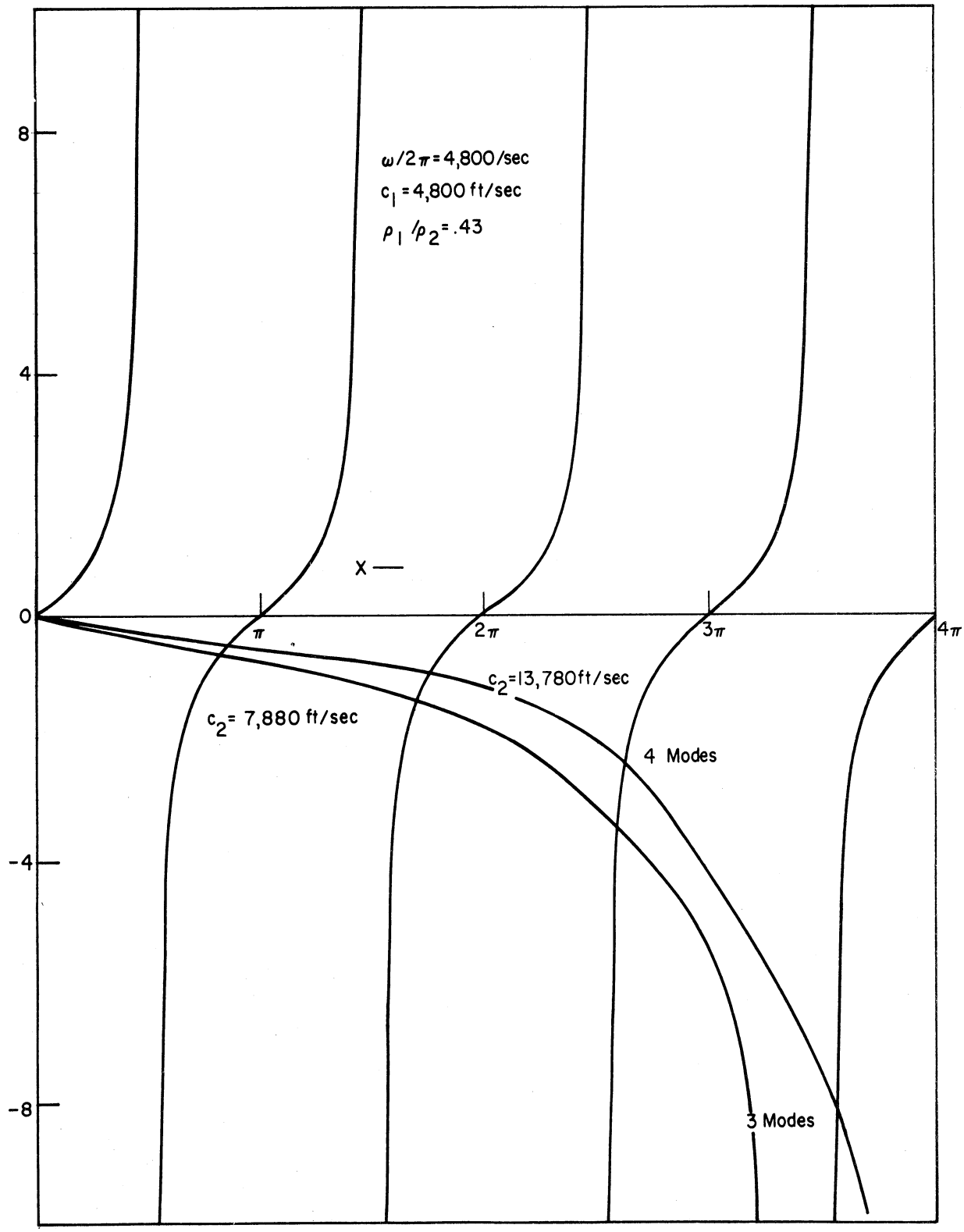

Fig. 7. Positioning of roots x_n for the two fluid case for different values of c_2.

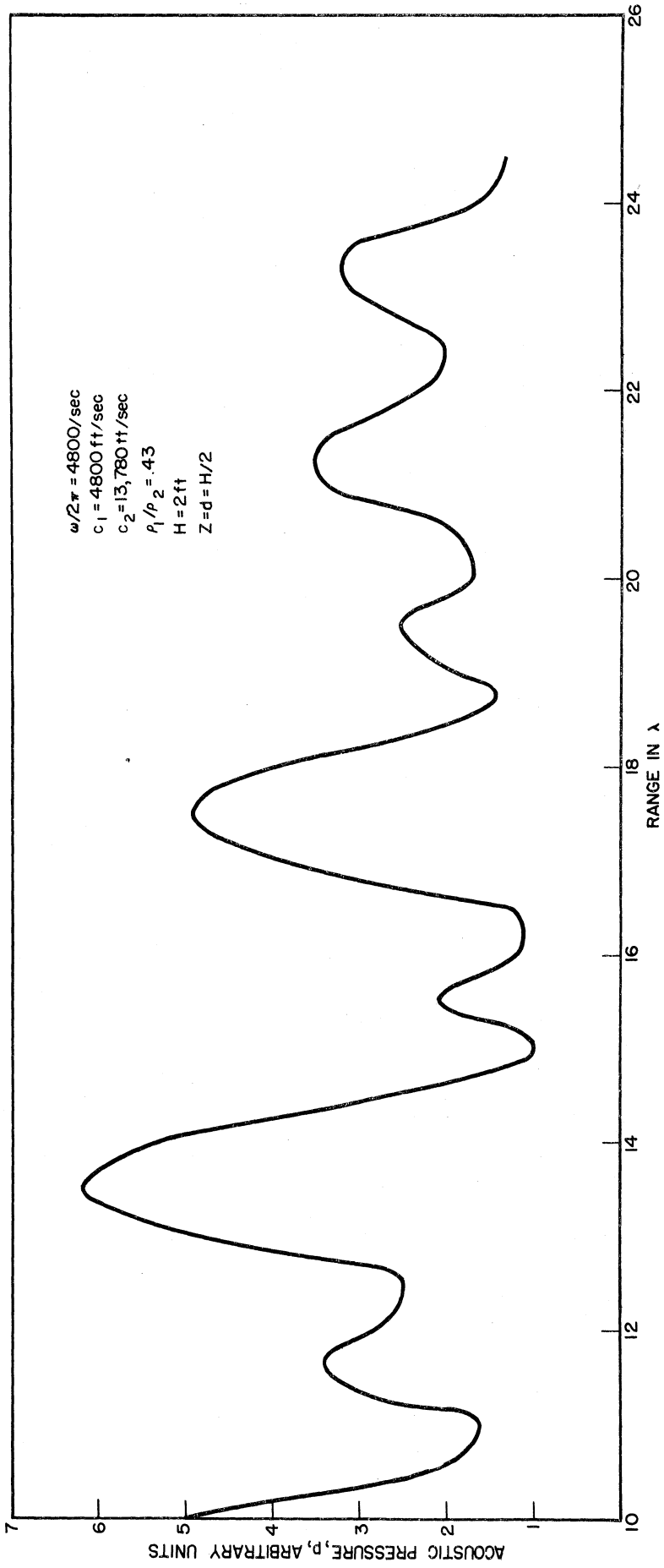

Fig. 8. Calculated acoustic pressure variation with range for a two fluid model.

there are no real roots. The positioning of the roots of Eq. (6) is illustrated in Fig. 7 for a single value of ω and two different values of c_2. In this figure the function

$$-\frac{x}{Hb}\,\frac{1}{\left(\omega^2/c_1^2 - x^2/H^2 - \omega^2/c_2^2\right)^{1/2}}$$

is plotted against x. The function $\tan x$ is also plotted and the points at which the curves cross give the roots x_n of the equation.

It suffices to compute the right hand side of Eq. (6) for a single frequency ω_0. For if one denotes the right hand side of Eq. (6) by $f(\omega,x,c_1,c_2)$ then $f(\alpha\omega_0,\alpha x,c_1,c_2) = f(\omega_0,x,c_1,c_2)$. By using this relationship, curves for different frequencies may be plotted with a minimum of effort.

It is clear from Fig. 7 that for c_2 sufficiently large compared to c_1 there will be as many real roots for a fluid bottom as there are for a rigid bottom. When this happens the pressure amplitude versus range curves for the two cases will be quite similar. Figure 8 shows a plot of pressure versus range for a two fluid case. The frequency chosen was 4800 cps. The density ratio ρ_1/ρ_2 was taken to be 0.43, a value which corresponds to the ratio of the density of water to that of concrete. The velocity c_2 was chosen to be 13,780 ft/sec, a value which corresponds to the compressional wave velocity for a typical concrete sample. The value of c_1 was chosen to be 4800 ft/sec. This last figure is roughly the value of the speed of sound in water. For the case chosen the branch line integral was found at a range of 10 ft to be much smaller in magnitude than the propagating modes. The pattern in Fig. 8 is therefore due to the interference of the four propagating modes. There is a marked similarity between the pattern of Fig. 8 and that of Fig. 3 which may be attributed to the fact that the number of propagating modes is the same for the two cases and that the values of corresponding wave numbers are quite close.

By comparison of Eqs. (5), (6), and (3) we see that if we let $b = \rho_1/\rho_2$ approach zero in Eqs. (5) and (6) the two fluid case solution reduces to that of the rigid bottom. Hence the latter may be considered to be a special case of the former.

The Solid Elastic Bottom Model - The elastic bottom model differs from the two fluid case in that the bottom is now to be thought of as being capable of transmitting shear waves. We shall in the following let c_c denote the velocity of the compressional wave in concrete and let c_s denote the velocity of the shear wave in concrete. It is also convenient to use the Lamé constants λ and μ, in terms of which c_c and c_s may be written as:

$$c_c = \sqrt{\frac{\lambda + 2\mu}{\rho_2}} \quad ; \quad c_s = \sqrt{\frac{\mu}{\rho_2}} \, .$$

The velocity of sound in the top fluid layer we shall denote by c_1 and the density of the top layer by ρ_1. Although it is still possible to describe the physical situation in the upper fluid layer by means of a scalar potential, in the bottom it is necessary to use both a scalar and a vector potential. We shall not enter here into the details of the solution but shall record the appropriate solution for the upper layer. The details of the derivation are to be found in reference (3). (The geometry of the situation is depicted in Fig. 9.)

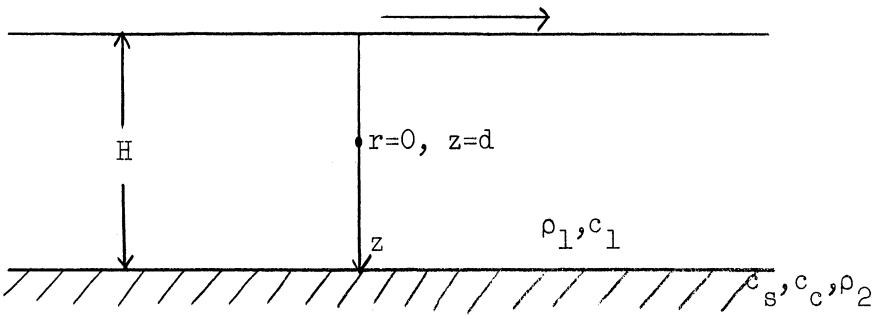

Fig. 9. The Geometrical Picture for the Solid Elastic Bottom Model.

The integral representation of the scalar potential ψ in the liquid layer has the form:

$$\psi = \begin{cases} 2e^{i\omega t} \int J_0(kr)(\sin\beta_1 z) \frac{k}{} \frac{Q\cos\beta_1(H-d) - P\sin\beta_1(H-d)}{Q(\cos\beta_1 H) - P\sin\beta_1 H}\, dk , \\ \qquad\qquad 0 \leq z \leq d \quad ; \\ 2e^{i\omega t} \int J_0(kr) \frac{k}{\beta_1} \sin\beta_1 d \frac{Q\cos\beta_1(H-z) - P\sin\beta_1(H-z)}{Q\cos\beta_1 H - P\sin\beta_1 H}\, dk , \\ \qquad\qquad d \leq z \leq H \quad ; \end{cases} \tag{7}$$

where $P = -\omega\beta_c k_s^2/\beta_1$,

$$Q = \frac{i}{\omega\rho_1}\left[2\lambda k_c^2(k^2-\beta_s^2) + 2\mu\left\{\beta_c^2(k^2-\beta_s^2) - 2\beta_s\beta_c k^2\right\}\right] ,$$

and

$$\beta_1 = \begin{cases} \sqrt{k_1^2 - k^2} & k < k_1 \qquad (k_1 = \omega/c_1), \\ -i\sqrt{k^2 - k_1^2} & k > k_1 \quad ; \end{cases}$$

$$\beta_c = \begin{cases} \sqrt{k_c^2 - k^2} & k < k_c \qquad (k_c = \omega/c_c), \\ -i\sqrt{k^2 - k_c^2} & k > k_c \quad ; \end{cases}$$

$$\beta_s = \begin{cases} \sqrt{k_s^2 - k^2} & k < k_s \qquad (k_s = \omega/c_s), \\ -i\sqrt{k^2 - k_s^2} & k > k_s \quad . \end{cases}$$

Before going on to write the normal mode form of the solution which is obtained by transforming these integrals into sums of residues of poles and branch line integrals, we note the above expression for ψ reduces to the corresponding expression for ψ for the two fluid case when $\mu \to 0$. Hence the elastic bottom colution contains the solutions of the two previous problems as special cases.

It is seen that the integrands of Eq. (7) have two branch points, one at $k = \omega/c_s$ and one at $k = \omega/c_c$. Hence upon transformation of the

integrals of Eq. (7) to obtain the normal mode form of the solution, one obtains in addition to the normal mode series two branch line integrals. One of these extending from $k = \omega/c_s$ to $k = \omega/c_s - i\infty$ and the other from $k = \omega/c_c$ to $k = \omega/c_c - i\infty$. The following is the asymptotic form of the solution represented as normal modes. It is valid for large $kr \gg 1$, and for $0 \leq z \leq H$:

$$\psi = e^{i\omega t}\left\{ -2\pi i \sum_{k_n} \frac{e^{-ik_n r + i\pi/4} \sin \beta_{1n} z \sin \beta_{1n} d}{\left[H + \frac{\frac{\partial Q}{\partial k}\cos \beta_1 H - \frac{\partial P}{\partial k}\sin \beta_1 H}{Q \sin \beta_1 H + P \cos \beta_1 H}\right]_{k=k_n} \sqrt{\frac{\pi}{2} k_n r}} \right.$$

$$+ \frac{e^{-ik_c r}}{(k_1 r)^2} \frac{2i \rho_1 \omega^4/c_s^2 k_c \sin(\alpha_c k_1 z) \sin(\alpha_c k_1 d)}{\alpha_c^2 \cos^2(\alpha_c H k_1) \left[\lambda(k_c^2(2k_c^2 - k_s^2))\right]} \qquad (9)$$

$$\left. + \frac{e^{-ik_s r}}{k_1^2 r^2} \frac{\sin(\alpha_s k_1 z)\sin(\alpha_s k_1 d) i\, 8k_s^5 (k_c^2 - k_s^2) \mu/\rho_1}{\alpha_s^2 \left[a'^2 \cos^2(\alpha_s H k_1) - \sin^2(\alpha_s H k_1) c'^2 + (\sin \alpha_s H k_1)(\cos \alpha_s H k_1) a' c'\right]_{k=k_s}} \right\}.$$

The last two terms in the above expression represent the two branch line contributions. These expressions for the branch contributions are valid providing we are removed from the zeros of the denominators. The form used for the branch line calculation is valid providing $c_1 < c_s < c_c$. This is true in the cases of greatest interest to us. The symbols Q and P are as defined in Eq. (8). In addition we have the following definitions,

$$a = \frac{i}{\omega\rho}\left[\lambda k_c^2(k^2 - \beta_s^2) + 2\mu\left\{\beta_c^2(k^2 - \beta_s^2)\right\}\right],$$

$$\mathcal{C} = \frac{i}{\omega\rho}\left[-2\beta_s k^2 2\mu\right],$$

$$\mathcal{A} = -\omega k_s^2/\beta_1,$$

$$a' = \frac{i}{\omega\rho_1}\left[\lambda k_c^2(k^2 - \beta_s^2) + 2\mu\left\{\beta_c^2(k^2 - \beta_s^2)\right\}\right],$$

$$\alpha_c = \sqrt{1 - c_1^2/c_c^2} \quad ,$$

$$\alpha_s = \sqrt{1 - c_1^2/c_s^2} \quad ,$$

$$\zeta' = -\frac{i}{\omega\rho_1} 4\beta_c k^2 \quad , \quad \text{and}$$

$$c' = -\omega\beta_c k_s^2/\beta_1 \quad .$$

The values of k_n which appear in the normal mode series are the roots of the transcendental equation $Q/P - \tan \beta_1 H$. The real roots k_n of this equation occur for $k_1 > k_n > k_s > k_c$. The period equation may be written more explicitly as:

$$\tan \beta_1 H = \frac{\beta_1}{b} \left[4 \left(k^2 - k^2\right)^{1/2} \frac{k^2}{k_s^4} - \frac{\left(1 - \frac{2k^2}{k_s^2}\right)^2}{\left(k^2 - k_c^2\right)^{1/2}} \right]$$

where $k_s = \omega/c_s$ and $k_c = \omega/c_c$ as above. Making the substitution $x = \beta_1 H$ the equation above may be written as:

$$\tan x = \frac{x}{bH} \left[4 \left(\omega^2/c_1^2 - \omega^2/c_s^2 - x^2/H^2\right)^{1/2} \frac{(\omega^2/c_1^2 - x^2/H^2)}{k_s^4} \right.$$

$$\left. \frac{\left[1 - 2(\omega^2/c_1^2 - x^2/H^2)/k_s^2\right]^2}{\left(\omega^2/c_1^2 - \omega^2/c_c^2 - x^2/H^2\right)^{1/2}} \right]$$

Figure 10 exhibits the positioning of the roots x_n of the above equation for various values of c_c and c_s. For c_s and c_c both sufficiently high there will be as many real modes as for the rigid bottom case for the same angular frequency ω and depth H. In some cases there will be one more mode than for the rigid bottom. In such a case two closely spaced elastic bottom modes will appear and correspond to a single rigid bottom mode. Figures 11, 12, and 13 are plots of the acoustic pressure versus range for an

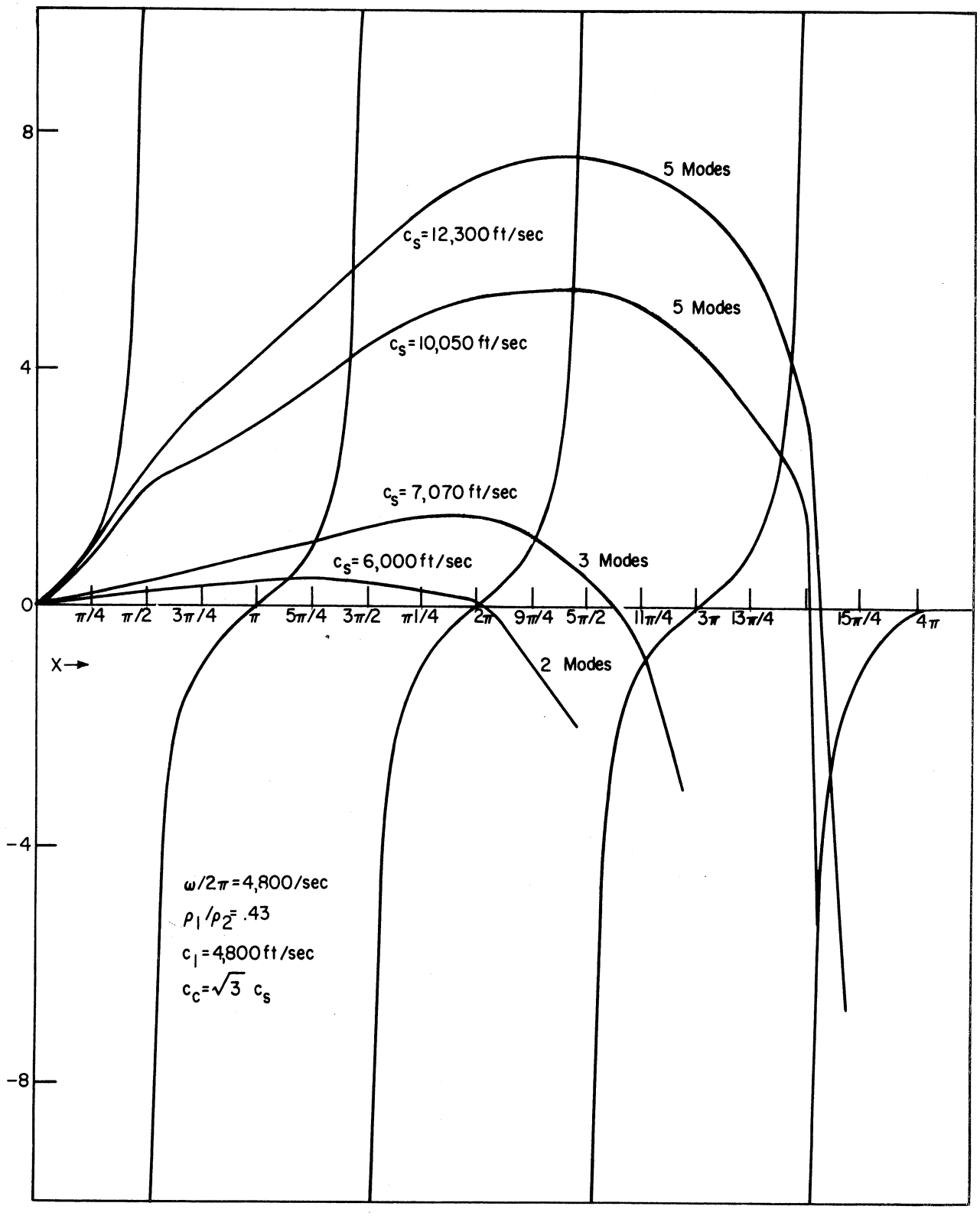

Fig. 10. Positioning of roots x_n for the elastic bottom period equation.

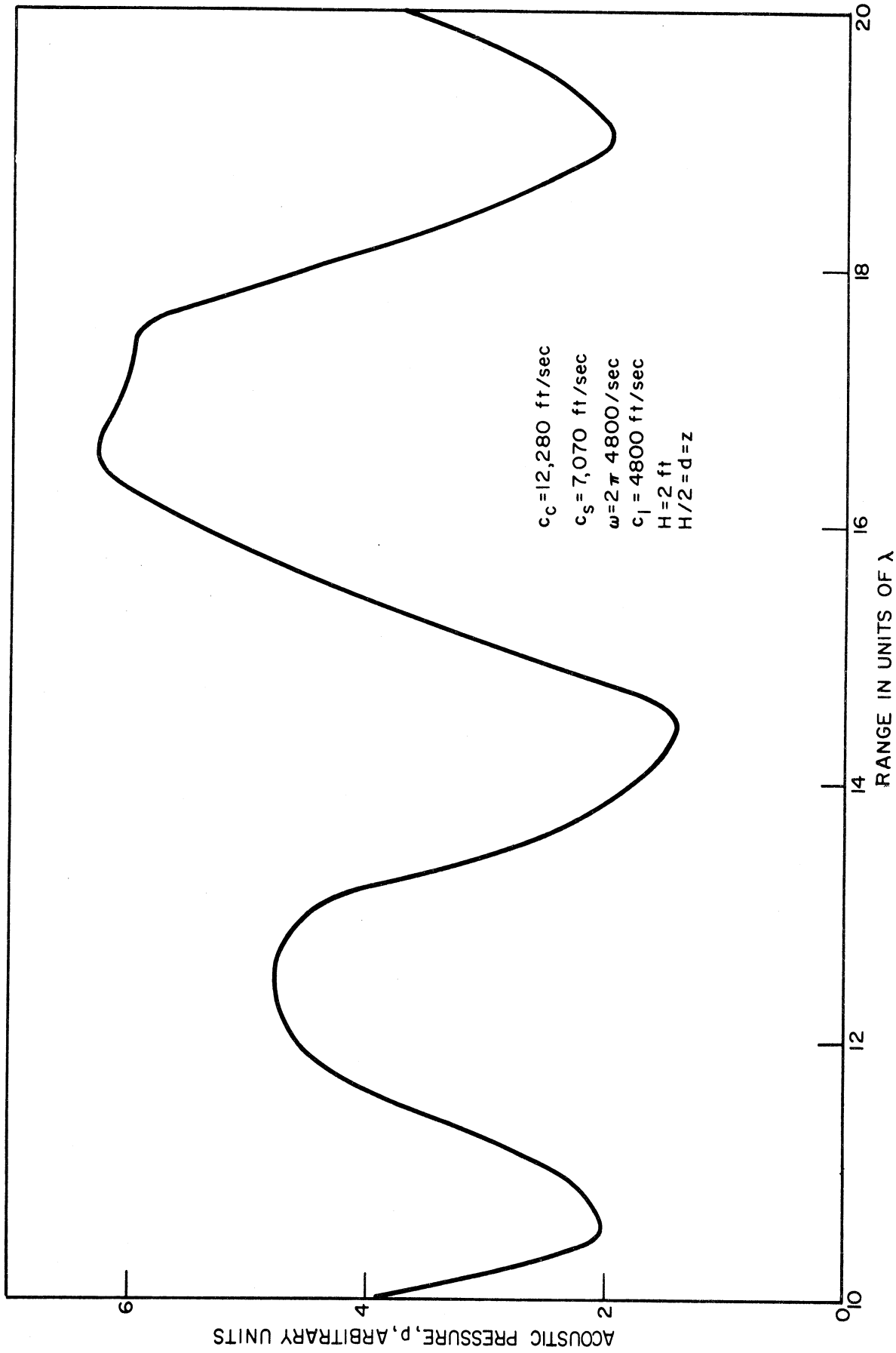

Fig. 11. Calculated acoustic pressure variation with range for an elastic bottom model. c_c = 12,280 ft/sec, c_s = 7070 ft/sec.

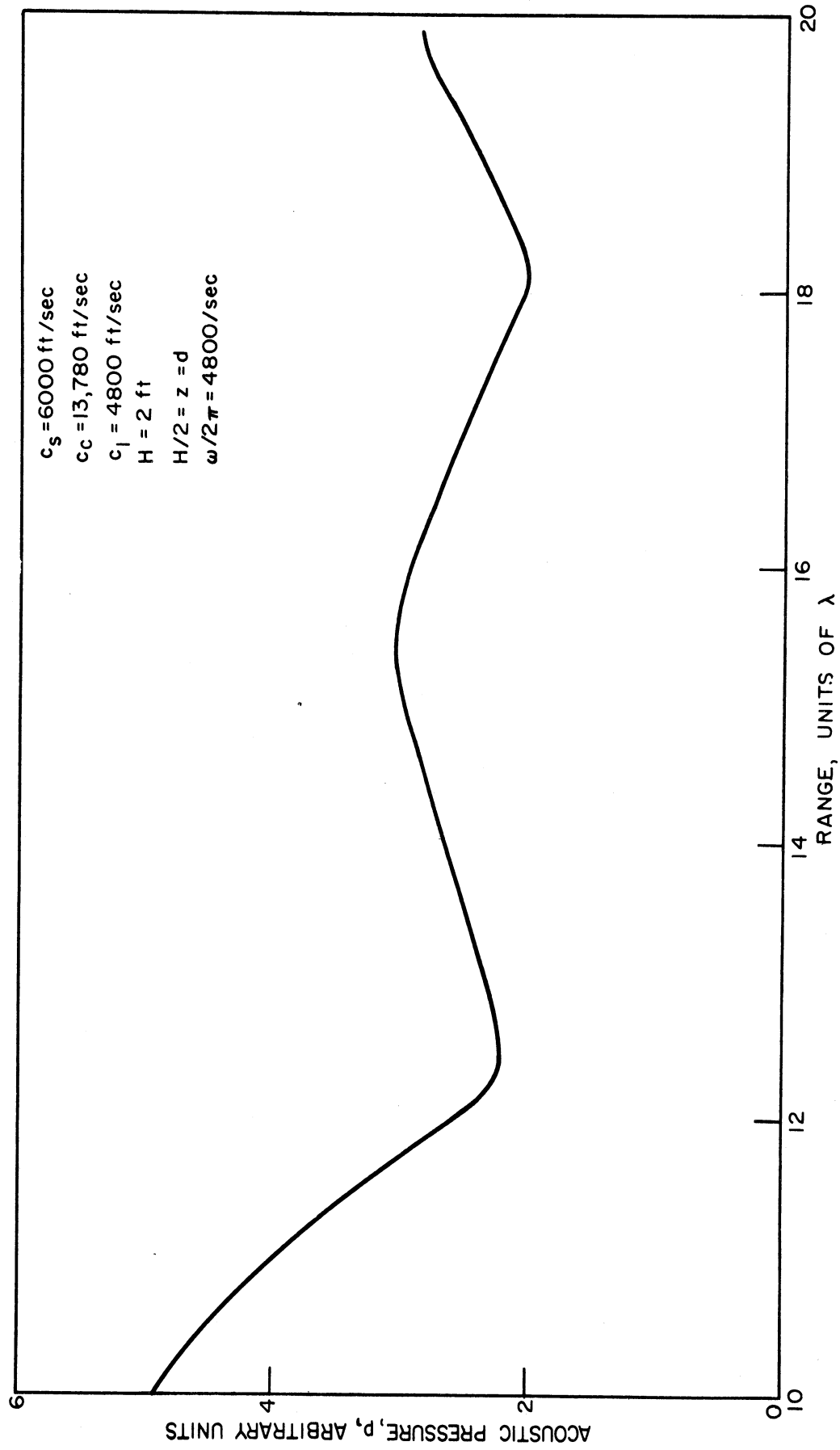

Fig. 12. Calculated acoustic pressure variation with range for an elastic bottom. c_c = 13,780 ft/sec, c_s = 6000 ft/sec.

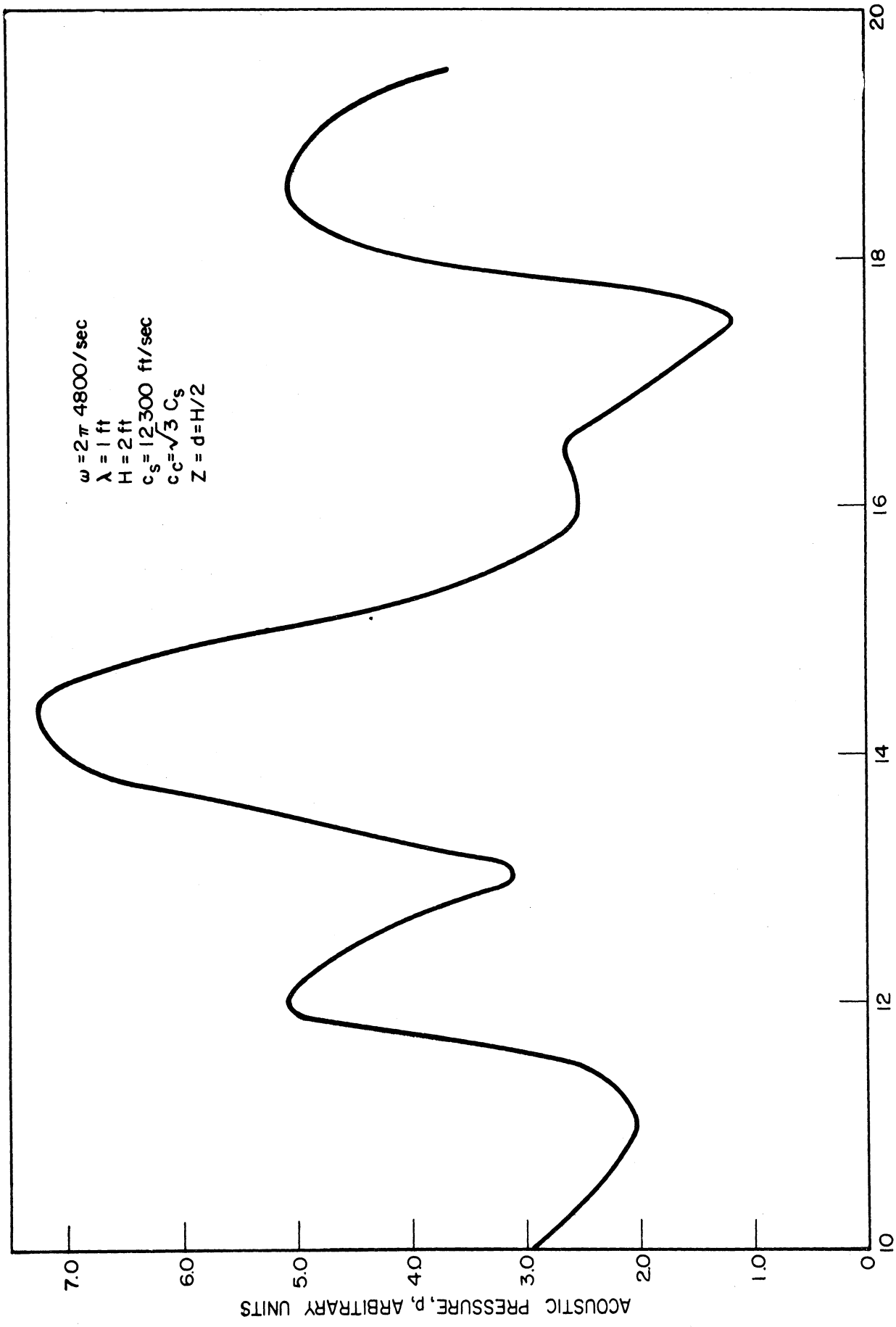

Fig. 13. Calculated acoustic pressure variation with range for an elastic bottom. $c_c = \sqrt{3}\, c_s$, c_s = 12,300 ft/sec.

elastic solid bottom. Figures 12 and 13 were plotted for values of c_l, c_s, and c_c which might be typical of a water layer over a concrete bottom. The frequency chosen and the depth to wave length-in-water ratio was the same as for Fig. 3. For the values of c_s and c_c used in calculating the pressure pattern for these graphs there were found to be fewer modes than for the corresponding rigid bottom case. This was due to the relatively low speeds used for the shear wave velocity. The pattern computed is quite unlike that of Fig. 3 which exhibits the rigid bottom results for the corresponding case, i.e. for the same frequency and depth-to-wave length ratio. In Fig. 13 acoustic pressure versus range was plotted using sufficiently high bottom speeds so that five propagating modes appeared, two of which corresponded to a single rigid bottom mode. At these speeds the pattern is similar to the rigid bottom pattern plotted in Fig. 3. It should be emphasized that the high bottom speeds used in calculating the pressure pattern for this graph are not those commonly associated with concrete.

Summary and Conclusion to Section 3.1.1.

The normal mode forms of the solution for a point source liquid layer over 1) a rigid bottom, 2) a fluid bottom, and 3) an elastic solid bottom have been presented and the results of calculations based on these models have been shown. All three models for ranges large compared to the wave length yield a scalar potential of the form:

$$\psi \cong e^{i\omega t} \sum \alpha_n(\omega, H, c_i) \frac{e^{-ik_n r}}{\sqrt{k_n r}} \sin \beta_n d \sin \beta_n z \qquad 0 \le z \le H \tag{9a}$$

where α_n is an amplitude factor. For the three models α_n are different functions of the physical parameters which describe the problem. The roots

k_n for the three models are determined by the three period equations

1) Rigid bottom --

$$\tan x_n = \infty$$

where $$x_n = H\sqrt{\omega^2/c_1^2 - k_n^2} = \beta_n H .$$

2) Two fluid --

$$\tan x_n = \frac{x_n}{Hb}\left(\frac{1}{\sqrt{k_n^2 - k_c^2}}\right)$$

3) Elastic solid bottom --

$$\tan x_n = \frac{x_n}{Hb}\left\{-\frac{(1 - 2k_n^2/k_s^2)^2}{\sqrt{k_n^2 - k_c^2}} + \frac{4k_n^2}{k_n^4}\sqrt{k_n^2 - k_s^2}\right\}$$

The real roots k_n for the three cases occur for the following ranges of the parameters (assuming $c_1 < c_s < c_c$) :

1) $\omega/c_1 > k$,

2) $\omega/c_1 \geq k > \omega/c_2$,

3) $\omega/c_1 > k > \omega/c_s > \omega/c_c$.

These last conditions correspond to the fact that the non-propagating modes correspond to radiation moving at angles greater than the critical angles associated with the bottom. The fluid and elastic bottom cases are characterized by having in addition to the normal modes, branch line integral contributions which, however, vanish at large distances as $1/r^2$ (compared with $1/r^{1/2}$ for the propagating modes).

Asymptotic formulas for the branch line integrals have been presented in Section 3.1.1; from these the magnitude of the branch line contribution may be determined at large ranges.

3.1.2. The Propagation of Pulses

In the preceding section the normal mode form of the solution was presented for a time harmonic pulse. We shall now briefly discuss distrubances with other types of time dependence.

An Approximate Method Using Normal Modes - First consider an approximate treatment of the response to a pulse which may be represented by a Fourier transform, $g(\omega)$, which peaks at the frequency ω_0. Let us express the original excitation of the medium as $e^{i\omega_0 t} f(t)$ where $f(t)$ is the envelope of the pulse.

The response $R_n(\omega)$ of a mode to this excitation function may be written, (see Eq. (92)):

$$R_n(\omega) = \frac{1}{\sqrt{2\pi}} \int_{\omega_0 - \frac{\Delta\omega}{2}}^{\omega_0 + \frac{\Delta\omega}{2}} \alpha_n(\omega) \frac{e^{i(\omega t - k_n r)}}{\sqrt{k_n r}} \left[g(\omega) \sin\beta_n z \sin\beta_n d \right] d\omega \quad (10)$$

when $kr >> 1$. Assuming $\alpha_n(\omega)$, $\sqrt{k_n}$, and β_n slowly varying functions of ω over the range $\omega_0 - \frac{\Delta\omega}{2} < \omega < \omega_0 + \frac{\Delta\omega}{2}$ we have:

$$R_n(\omega) \cong \alpha_n(\omega_0) \sin\beta_{n0} z \sin\beta_{n0} d \frac{1}{\sqrt{2\pi}} \int_{\omega_0 - \frac{\Delta\omega}{2}}^{\omega_0 + \frac{\Delta\omega}{2}} e^{i(\omega t - k_n r)} g(\omega) d\omega$$

Expanding k_n about k_{n0} we have to a first approximation:

$$k_n(\omega) \cong k_{n0} + (\omega - \omega_0) \left. \frac{dk_n}{d\omega} \right|_{\omega = \omega_0} , \quad (10a)$$

where $k_{n0} = k_n(\omega_0)$ and $\beta_{n0} = \beta_n(\omega_0)$.

Hence

$$R_n(\omega) \cong e^{i(\omega_0 t - k_{n0} r)} \frac{\alpha_n(\omega_0) \sin\beta_{n0} z \sin\beta_{n0} d}{\sqrt{k_{n0} r}} \frac{1}{\sqrt{2\pi}} \int_{\omega_0 - \frac{\Delta\omega}{2}}^{\omega_0 + \frac{\Delta\omega}{2}}$$

$$e^{i \left[(\omega - \omega_0) t - (\omega - \omega_0) \left. \frac{dk_n}{d\omega} \right| r \right]} g((\omega) d\omega$$

Since

$$\frac{1}{\sqrt{2\pi}} \int_{\omega_0 - \frac{\Delta\omega}{2}}^{\omega_0 + \frac{\Delta\omega}{2}} g(\omega)\, e^{i(\omega - \omega_0)\left(t - \left.\frac{dk_n}{d\omega}\right| r\right)} d\omega =$$

$$e^{i\omega_0 \left.\frac{dk_n}{d\omega}\right| r} f\left(t - \left.\frac{dk_n}{d\omega}\right|_{\omega=\omega_0} r\right) ,$$

we see,

$$R_n(\omega) = \frac{e^{i\left(\omega_0 t - k_{n0} r + \omega_0 \left.\frac{dk_n}{d\omega}\right| r\right)}}{\sqrt{k_{n0} r}} \alpha_n(\omega_0)(\sin\beta_{n0} z)(\sin\beta_{n0} d) f\left(t - \left.\frac{dk_n}{d\omega}\right|_{\omega=\omega_0} r\right) \tag{11}$$

The result may be expected to hold when (see Eq. (10a)),

$$\left| \left.\frac{d^2k}{d\omega^2}\right|_{\omega=\omega_0} \right| (\Delta\omega)^2 \, r << 1 \quad .$$

From Eq. (11) it is seen that one can think of the response for each mode as being the original excitation function $f(t)$ reproduced in shape and travelling through the medium with the group velocity

$$v_{group} = \frac{1}{\left.\frac{dk}{d\omega}\right|_{\omega=\omega_0}} = \left(\frac{d\omega}{dk_n}\right)_{k=k_{n0}} .$$

Due to the fact that the different modes have different group velocities the original pulse will be elongated and distorted. The group velocities associated with the various modes may be computed if one knows the period equation. We have for the three models discussed in Section 3.1.1 the following group velocity formulas obtained by implicit differentiation of the period equations.

1) Rigid Bottom

$$v_g v_p = c^2$$

where v_g is the group velocity and v_p is the phase velocity;

2) Two Fluid

$$v_g v_p = \frac{\alpha + \gamma}{\frac{\alpha}{c_1^2} \quad \frac{\gamma}{c_c^2}}$$

where $\alpha = H^2 \left(\frac{\sec^2 x_n}{x_n} - \frac{\tan x_n}{x_n^2} \right)$, $\gamma = \frac{x_n}{bH\beta_{cn}^3}$,

and $\beta_{cn} = \sqrt{k_n^2 - \omega^2/c_c^2}$;

3) Elastic Solid Bottom

$$v_{group}\, v_{phase} = \frac{\alpha + \overline{\gamma} + \delta + \epsilon + \eta}{\frac{\alpha}{c_1^2} + \frac{\gamma}{c_c^2} + \frac{\delta}{c_s^2} + \frac{\epsilon}{v_{ph}^2} + \frac{2\eta}{v_{ph}^2}}$$

where $\overline{\gamma} = \frac{x_n \left(1 - \frac{2k_n^2}{k_s^2}\right)^2}{bH\,\beta_{cn}^3}$, $\delta = \frac{4x_n k^2}{bH\beta_{sn}k_s^4}$,

$$\epsilon = \frac{8x_n \left(1 - \frac{2k^2}{k_s^2}\right)}{bH\,\beta_{cn}k_{sn}^2} \quad , \quad \eta = \frac{x_n 8\beta_{sn}}{bH\,k_s^4} \quad ,$$

$$\beta_{sn} = \sqrt{k_n^2 - k_s^2} \quad , \quad \beta_{cn} = \sqrt{k_n^2 - k_c^2} \quad .$$

By the use of velocities computed from these formulas one may calculate the spreading of the initial pulse. Actually at ranges of interest here the results will be only qualitatively correct as we shall see from computation based on the image series form of the solution. Using the above formulas for the group velocities, calculations have been made to show the spreading of

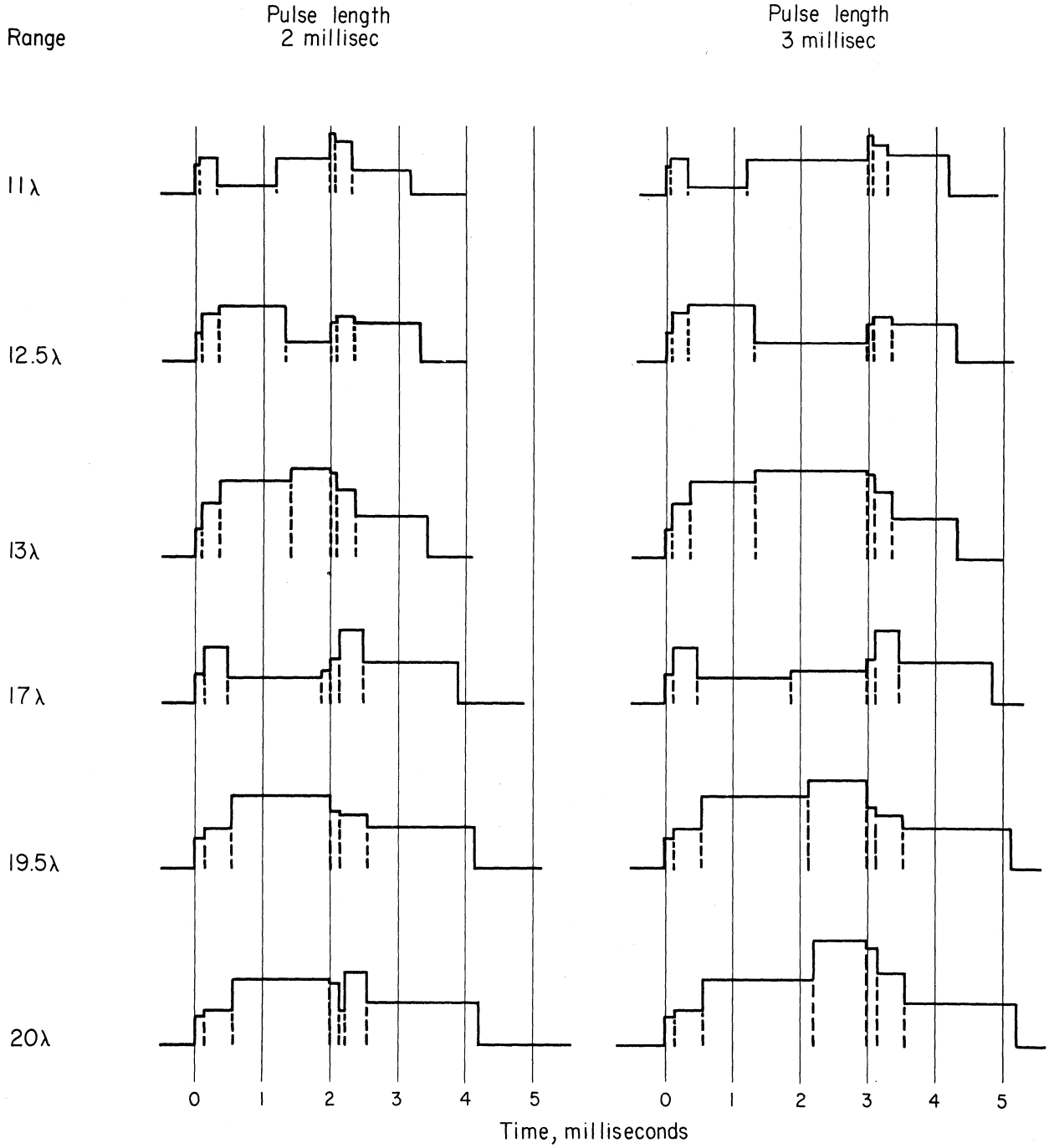

Fig. 14. Calculated pulse shapes using a normal mode first order approximation for a rigid bottom.
$\omega = 9600/2\pi$ radians/sec, $\lambda = 0.5$ ft, $H = 2\lambda$.

the pulse for the case of a rigid bottom. It was assumed that the pulse had a square envelope. The results are exhibited in Fig. 14. At each range the fastest mode arrives first and then in succession the other modes arrive to interfere with it. The arrival time for each mode was computed using the appropriate group velocity. One can see that if the pulse length is short enough, the first mode may cut off before the arrival of the slow modes. In order to obtain the continuous wave result the pulse length must be long enough so that at the ranges of interest there is a region of the received pulse in which all of the important modes interfere. For the parameters chosen there are at most four modes propagated. The cut-on or cut-off of the successive modes are indicated by changes in the pulse amplitude.

Image Series Solution -- An image series representation of the solution lends itself more readily to the integration of the finite time pulse at moderate ranges.

For the case of the rigid bottom the image series may be obtained directly as follows:

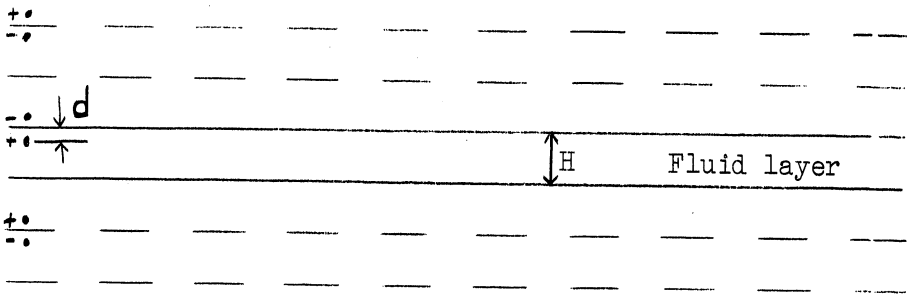

Fig. 15. Location of images for a fluid layer bounded on the upper side by a free surface and on the lower by a rigid surface.

We consider a source at a depth d in a fluid layer of depth H bounded on the one side by a free surface and on the other by a rigid surface. Then the boundary conditions to be satisfied by the scalar potential ψ are

$$\frac{\partial \psi}{\partial n} = 0 \quad \text{at} \quad z = H ,$$

$$\psi = 0 \quad \text{at} \quad z = 0 .$$

Consider the point source solution to the Helmholtz equation, $\psi = \frac{e^{-ikR_0}}{R_0}$ with $k = \omega/c$ and where R_0 is distance of the field point (r,z) from the source i.e., $R_0 = \sqrt{r^2 + (z-d)^2}$. In order to satisfy the boundary conditions at $z = 0$ and $z = H$ we start with two images of the source, one in the upper surface and one in the lower surface. Labelling the fields corresponding to these images by ψ_1 and ψ_{-1}

$$\psi_1 = -\frac{e^{-ikR_1}}{R_1} \qquad \text{where} \quad R_1 = \left(r^2 + (z+d)^2\right)^{1/2}$$

$$\psi_{-1} = \frac{e^{-ikR_{-1}}}{R_{-1}} \qquad \text{where} \quad R_{-1} = \left(r^2 + (z-2H+d)^2\right)^{1/2} .$$

By continuing this process of imaging one arrives at the following series which satisfies the wave equation and all the boundary conditions of the problem and is therefore an exact solution to the problem:

$$\psi = e^{i\omega t} \sum_{n=-\infty}^{\infty} (-1)^n \left\{ \frac{e^{-i(\omega/c)\left(r^2+(z-2nH-d)^2\right)^{1/2}}}{\left(r^2 + (z-2nH-d)^2\right)^{1/2}} \quad \frac{e^{-i(\omega/c)\left(r^2+(z+2nH+d)^2\right)^{1/2}}}{\left(r^2 + (z+2nH+d)^2\right)^{1/2}} \right\} \tag{12}$$

For the special case of $z=d=H/2$ we obtain the following form,

$$\psi_{z=d=H/2} = e^{i\omega t} \sum_{n=-\infty}^{n=\infty} (-1)^n \left\{ \frac{e^{-i\omega/c\left(r^2+(2nH)^2\right)^{1/2}}}{\left(r^2 + (2nH)^2\right)^{1/2}} \right\} . \tag{13}$$

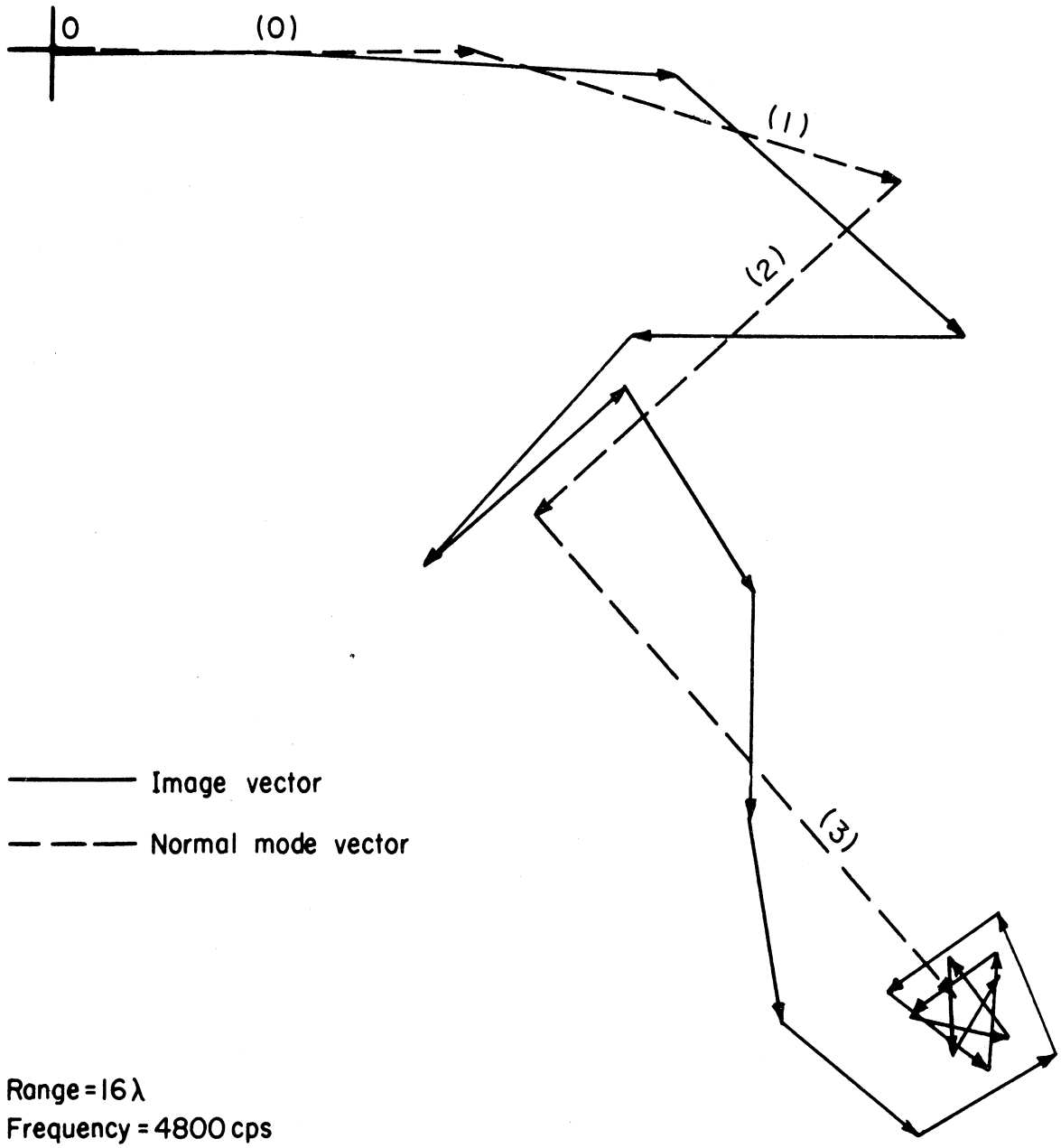

Fig. 16. Summation of the image and normal mode serials.

The image series is especially easy to use for non-periodic time excitations. Corresponding to a source excitation of the form $f(t)$ we have:

$$\psi = \sum_{n=-\infty}^{n=\infty} (-1)^n \left\{ \frac{f\left(t - \sqrt{r^2+(z-2nH-d)^2}/c\right)}{\left(r^2 + (z-2nH-d)^2\right)^{1/2}} \quad \frac{f\left(t - \sqrt{r^2+(z+2nH+d)^2}/c\right)}{\left(r^2 + (z-2nH+d)^2\right)^{1/2}} \right\}$$

Each term of the image series represents rays which have undergone a definite number of reflections from the top and bottom surfaces of the liquid layer. The image series includes all such rays. It is evident that for large ranges it converges slowly.

Figure 16 shows the relative rates of convergence of the image and normal mode series for the case $c = 4800$ ft/sec, $\omega = 4800\ 2\pi$/sec, $H = 2$ ft, and $d = z = H/2$, a case which we have alreasy considered using normal mode theory. The vectors drawn in heavy lines are the image contributions. The four dotted line vectors represent the four propagating normal modes. Thus even at the moderate range considered it is necessary to sum many more than four terms of the image series in order to get a good approximation to the sum of the image series. With increasing range the work involved in the summation of the image series increases rapidly.

Each normal mode represents the contribution of many images. This situation may be seen from the fact that the normal mode contribution of a mode to the field amplitude decreases as $\frac{1}{\sqrt{r}}$ whereas each image contribution decreases as $\frac{1}{r}$. In particular a normal mode may be thought of as representing the sum of groups of images which interfere constructively at the field point. Consider the case of a source and receiver at mid-depth where one may neglect the images (marked x in Figure 17) since these always cancel for $z=d=H/2$. One sees that the difference in phase of two rays arriving from images proceeding at an angle θ will upon arrival at the

field point be $4\pi \frac{H \cos \Theta}{\lambda} - \pi$. The condition for constructive interference is:

$$4\pi \frac{H \cos \Theta}{\lambda} - \pi = 2n\pi, \quad n = 0, 1, 2, \ldots.$$

or

$$\cos \Theta_n = \frac{2n+1}{4H} \lambda ,$$

and

$$\sin \Theta_n = (c/\omega) \left(\omega^2/c^2 - \frac{(2n+1)^2}{(2H)^2} \pi^2 \right)^{1/2} = \frac{\lambda}{2\pi} k_n ;$$

here k_n are the roots of the period equation for the rigid bottom. Thus a normal mode represents a group of constructively interfering rays from the images which rays travel at the angles Θ_n given by the above relationship.

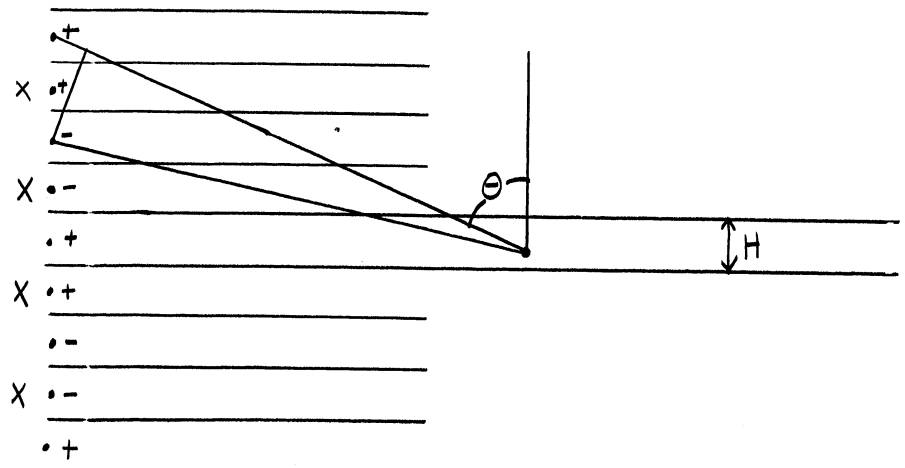

Fig. 17. Constructive interference of images to form modes for a rigid bottom.

The image series, although inconvenient for computational purposes when the range is very great is, however, ideally suited to the integration of finite time pulses for moderate ranges. If one has the patience, one may achieve the exact integration of the time pulse for the rigid bottom case. This has been carried out for a pulse with a rectangular envelope and the results are displayed in Fig. 18. A comparison is made in the figure with the treatment of the finite pulse by the approximate method using normal modes

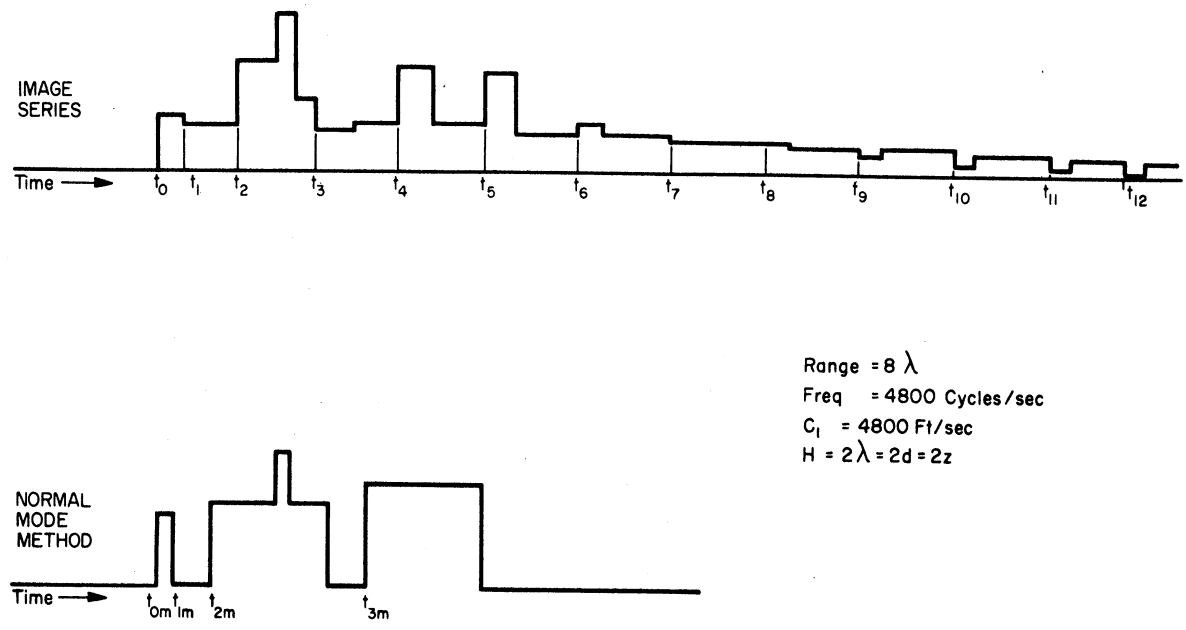

(a) Initial pulse length = 1 millisec

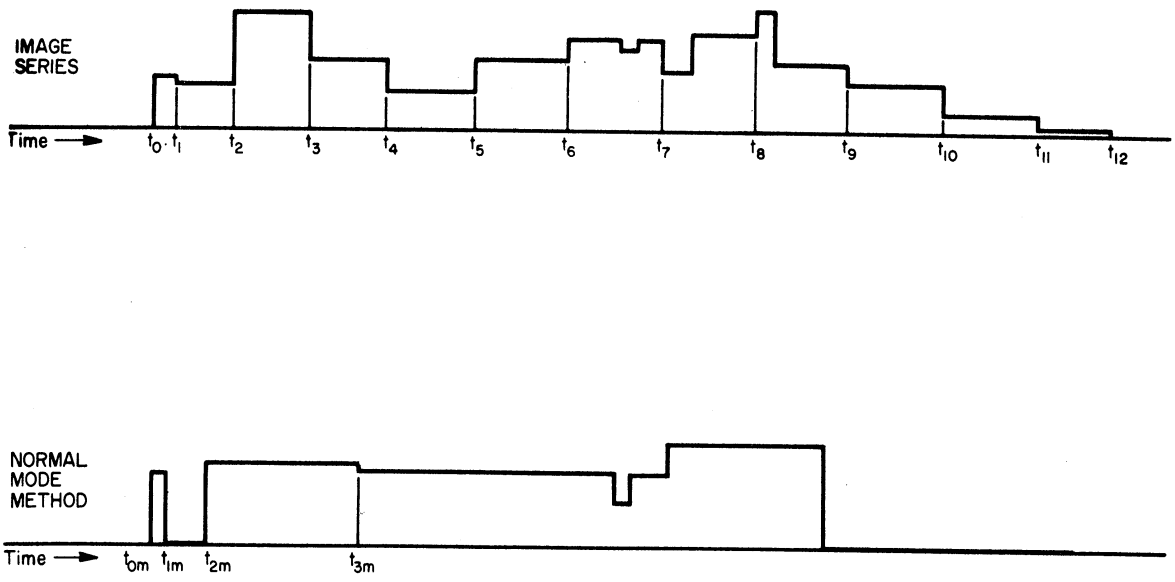

(b) Initial pulse length = 4 millisec

Fig. 18. A comparison of the integration of the time pulse by the image series and the approximate normal mode method.

described above. Although the normal mode treatment gives one an idea of the distortion of the original pulse it does not suffice to give the detailed picture which is obtained by summation of the image series. Here the discontinuities in pulse shape are due to the arrival of successive rays corresponding to different numbers of reflections from the top and bottom surfaces. As successive rays arrive one obtains successive approximations (see Fig. 16) to the amplitude of the scalar potential.

Pekeris[2] has derived an analogous ray series solution for the case of two fluids. Honda and Nakamura[4] deal with a corresponding series for the elastic solid bottom. For these two cases the plane wave reflection coefficient for the bottom appears in the ray series expressions. One finds that terms corresponding to multiple reflections from the bottom are multiplied by the corresponding powers of the reflection. In Fig. 19 is plotted the reflection coefficient as a function of angle of incidence for a plane wave incident upon an elastic bottom for values of c_c and c_s typical of concrete. This plot can be used in connection with the work cited to obtain the approximate image representation of the field for two fluid and fluid over elastic solid problems.

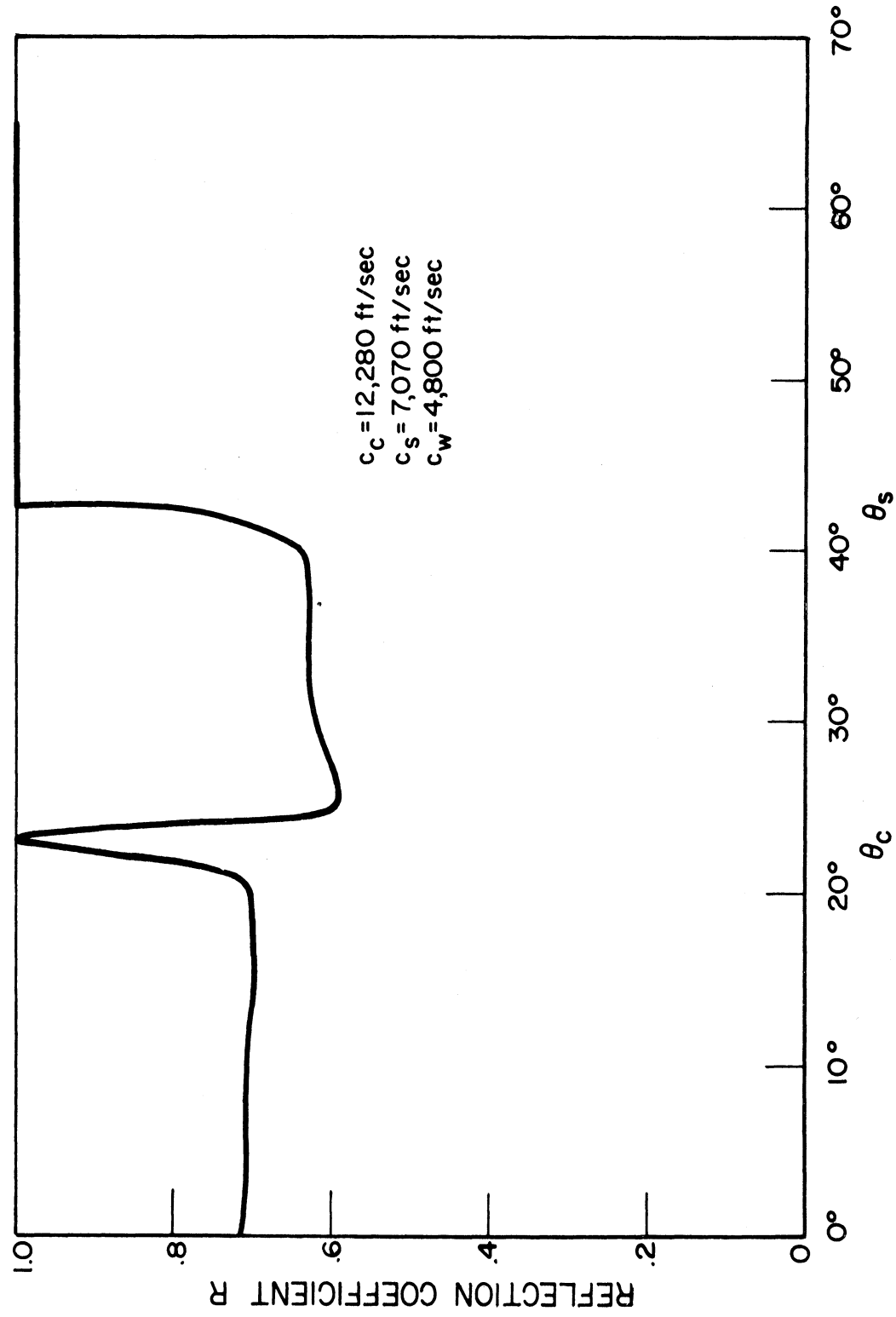

Fig. 19. Calculated amplitude reflection coefficient, R, for plane waves incident at an angle θ upon the plane interface between a fluid and an elastic solid.

APPENDIX

THE EFFECT OF THE FINITE THICKNESS OF THE CONCRETE ON THE PROPAGATION OF SOUND IN THE FLUID LAYER

A plane wave treatment allows one to quickly estimate the effect of the finite thickness of the bottom layer upon the propagation of sound in the top fluid layer. The normal mode problem for many plane layers has been solved by many investigators but the results are quite cumbersome to apply. Pekeris[2] for example treats the three-layer problem.

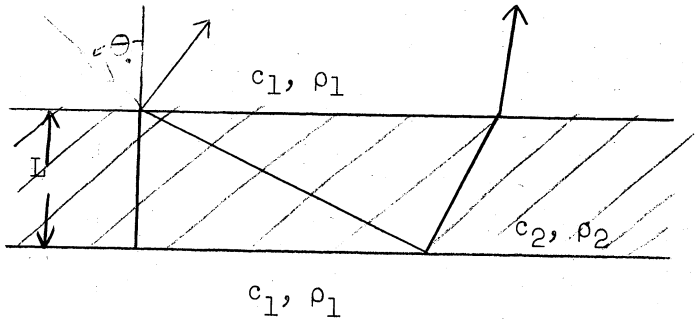

Fig. 20. Plane wave incident upon a fluid layer; c_2 = 12,800 ft/sec, c_1 = 4,800 ft/sec, ρ_1/ρ_2 = 0.43, and L = 6 inches.

One may, however, get an estimate of the effect of bottom thickness by supposing the incident field to consist of a plane wave. One calculates the plane wave reflection coefficient for those incident angles θ_n which correspond to the propagating modes for the case obtained by allowing $L \longrightarrow \infty$ and observes the magnitude of the reflection coefficient for the case of a finite second layer ($L < \infty$). If this is close to unity one concludes that though the modes may be shifted due to difference in phasing, their attenuation will be small.

The plane wave reflection coefficients for the situation depicted in Fig. 20 when the middle layer is a fluid, are shown in Table I.* The physical constants are those pertinent to the model experiment described in this report.

TABLE I
Amplitude Reflection Coefficients for Various Angles of Incidence

θ	A_r
84°	.99
68°	.99
51°	.98
29°	.97

One can see from this table that for a bottom characterized by a velocity c_2 in the neighborhood of that of concrete, the solution for the six inch bottom should be much the same as far as infinite layer since little energy is transmitted into the underlying regions.

---

* Constants used: c_1 = 4800 ft/sec.; c_2 = 13,000 ft/sec.; ρ_1/ρ_2 =0.43
L = 0.5 ft.

BIBLIOGRAPHY

1. Lamb, H., "On the Propagation of Tremors over the Surface of an Elastic Solid", Trans. Roy. Soc. 203A, p. 1 (London) (1904).

2. Pekeris, C.L., Propagation of Sound in the Ocean, Memoir 27, "Theory of Propagation of Explosive Sound in Shallow Water", Geological Society of America (1948) Baltimore, Maryland.

3. Press, F., and Ewing, M., "Propagation of Explosive Sound in a Liquid Layer Overlying a Semi-Infinite Elastic Solid", Geophysics 15, p. 426, (1950).

4. Honda and Nakamura, Bulletin of Science, Geophysics, University of Tohoku (1954).

3.2. EXPERIMENTAL INVESTIGATION OF THE PROPAGATION OF SOUND IN A SHALLOW WATER MODEL

J.E. Lesch and J.R. Frederick

A description of the several procedures used in the experimental pursuit of information concerning the propagation of sound in shallow water as modelled in large concrete tanks is given in this section.

The primary purpose of the experimental investigation thus far has been to explore the characteristics of the model. Before introducing additional complicating factors it appeared desirable to examine the simplest system available, and to investigate the extent to which the following factors might affect subsequent experiments:

1. elastic properties of the bottom
2. acoustic properties of the model
3. repeatability of the experiments.

In the preliminary phases of the model study programs reported here, two aspects have been particularly emphasized. One was that of comparing the results of experiments in the tank with those calculated theoretically on the basis of various simplifying hypotheses with the hope of finding the simplest mathematical model which would be useful. Secondly the effect of slight changes of the variables on the sound field has been examined.

3.2.1. Equipment and Techniques

The principal features of the apparatus and experimental procedures are described here. There is essentially nothing unique about either the equipment or techniques employed in the experiment. Possible exceptions are the use of tape recorded pulses for a signal source and one or two methods of treating the data.

A block diagram of the equipment is shown in Fig. 21. The variables associated with the tank in this experiment are water depth, projector and hydrophone depths, projector-hydrophone separation, sound frequency and orientation of the range with respect to the sidewalls. The effect of other parameters such as surface roughness and different bottom types will be examined in the future.

Both continuous-wave and pulsed signals are used. Except for the generation of the outgoing signal and the method of recording the received signal level, the same equipment is used for both techniques.

The pulses used in the experiments were first recorded on a magnetic tape using a high quality gating circuit designed and built by another research group at the University of Michigan. This device gates a c-w voltage to provide a pulse that cuts on and off at the axis crossing of the wave; the number of cycles in a pulse as well as the pulse repetition rate are readily controlled. A continuous loop carrying one or more of these recorded pulses is used as a source of signals. Pulse lengths of from one to fourteen milliseconds are available at repetition rates of from one to ten per second.

Most of the measurements have been made using a Bell Telephone Laboratories Type 1K projector and a Bell Telephone Laboratories Model 3A hydrophone. Both of these units have been obtained from the U.S.N. Underwater Sound Reference Laboratory. Some of the first experiments were performed using cylindrical barium titanate elements as projectors and hydrophones. The former were about 1-1/2 inch in diameter and the latter 1/4 inch in diameter.

Two tanks have been used. The dimensions of Tank 1 are 90 x 40 x 3.7 feet. Tank 2 shown in Fig. 22 is 95 x 53 x 3 feet deep. Gates in the tanks are provided for easy access of tractors or other vehicles used in handling various bottom materials. A wave-making machine is available which can produce

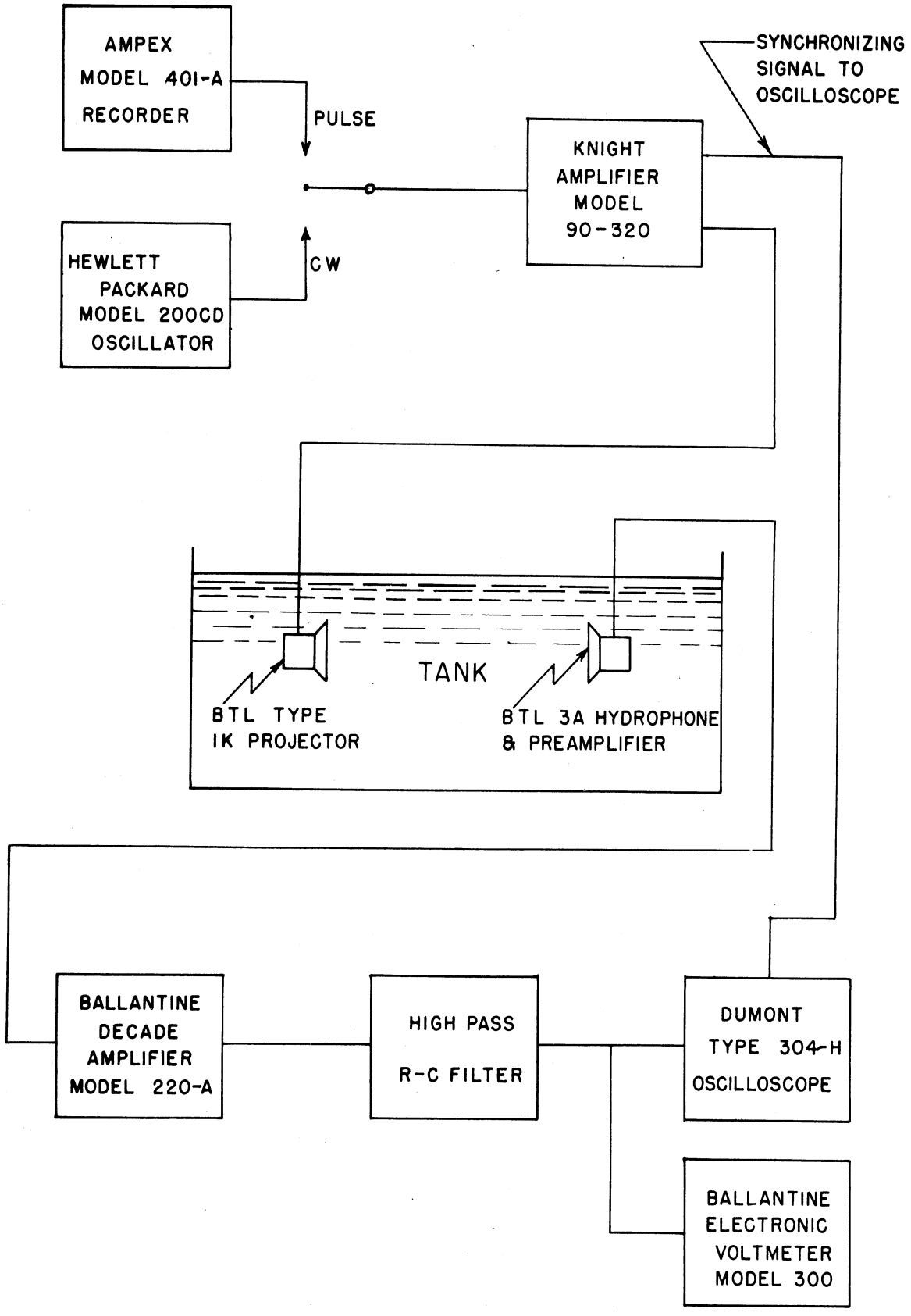

FIGURE 21. BLOCK DIAGRAM OF APPARATUS

Fig. 22. Photograph of tank 2. The electronic equipment is at the far end of the tank. The hydrophone is suspended from the trolley riding the track mounted adjacent to the catwalk.

waves of controlled frequency and amplitude. Plane wave fronts 20 feet or more in width can be produced.

3.2.2. Continuous-Wave Experiments

4Kcps -- The first c-w experiments were performed to determine the extent to which the tanks approximate an ideal situation, i.e. rigid bottom and no wall effects. It was decided to measure the pressure amplitude variation of the received signal as a function of range for a condition which could be treated without unreasonable difficulty using normal mode theory. The ratio of water depth to radiation wave length (H/λ) was fixed at a value of 2. Projector depth d and receiver depth h were held constant and equal to λ. Under the presumed ideal conditions four normal modes should be propagated.

The field has been measured in both tanks under these conditions employing the 1K projector and the 3A hydrophone as the receiver. Ranges employed were in general no greater than 30λ. A representative plot of the measured field is given in Fig. 23 and is compared with the theoretical field as calculated in section 3.1.1 for a rigid bottom condition. Since the theory becomes rather difficult at ranges less than 10λ or so, no calculations have been made in that region. An adjustment has been made in the mean level of the calculated curve to bring it to a level comparable with the experimental curve.

Several features of the experimental data should be noted.

1. In the range employed the plot compares most favorably with the rigid bottom calculation (as compared with the calculations of section 3.1.1 for the fluid and elastic bottoms).
2. The measured field shows an additional amplitude peak at the range of 25.5 feet (as compared with the rigid bottom calculation).

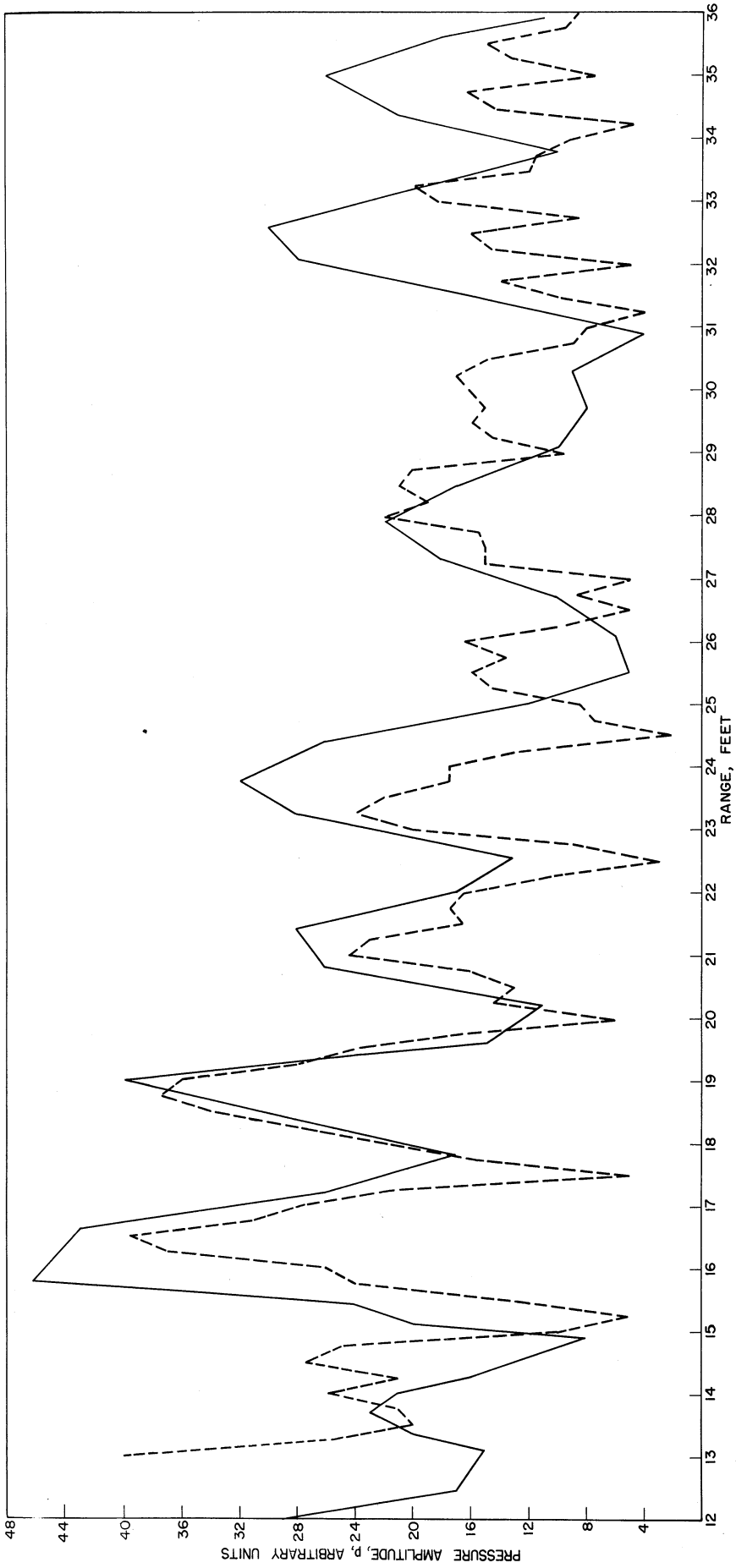

Fig. 23. Acoustic pressure variation with range. Frequency = 4 kcps, H/2 = h = d = λ. Theoretical curve is solid line. Measured curve is dashed line.

3. "Fine structure" in the amplitude increases with range with an indication that constructive interferences are occurring at range intervals of $\lambda/2$. (Some data not shown here indicate still further deterioration of the pressure field at greater ranges.)

With regard to statements 1 and 2 above it should be recalled that the calculated fields for rigid and fluid bottoms are not far different. A significant point is that both the rigid and fluid bottom calculations result in a field with four propagating modes. The elastic bottom calculation of Fig. 13 is based on certain assumed values of the compressional and shear wave velocities in the bottom, and at the frequency employed shows five propagating modes. Two of these correspond to the fourth rigid bottom mode. Although such a calculation has not yet been made, it is anticipated that a new calculation using the recently measured velocities of the bottom propagated waves will show closer agreement between the measured field and the elastic bottom calculation.

The above-mentioned fine structure on the experimental curve is barely noticeable at the shorter ranges and becomes increasingly prominent at the larger ranges. The peaks appear at intervals of 0.5 - 0.75 feet. Since the standard datum interval is 0.25 feet and $\lambda \approx 0.6$ feet, one deduces that the observed fine structure is caused by constructive interference at range intervals of $\lambda/2$.

If one examines amplitude versus range plots of data at values of h other than λ but under otherwise identical experimental conditions, one finds additional fine structure with a similar spacing of peaks. Between 7 feet (the shortest range of observation) and a range of about 25 feet the interference peak-to-trough amplitude difference is often up to one-half the total signal amplitude. Between the ranges of 25 and 40 feet the apparent $\lambda/2$ spaced interference peaks are significantly reduced both in number and

in relative amplitude. As the range is increased from about 40 to 55 feet (the largest range of observation) the interference tends to build up again.

The structure just described is superimposed on the apparent modal amplitude variations whose depth dependence is shown in section 3.1.1.

In attempting to offer a plausible explanation for the presence of this anomalous interference pattern, one can quickly eliminate the possibilities of side-wall and projector end-wall reflections. It is obvious that with the side walls located 26.5 feet away any interference by reflections from these walls would result in interference maxima at range intervals of somewhat greater magnitude and increasing spacing as the traverse range increased. On the other hand the projector end-wall reflection will be added to the direct path signal with a phase difference that remains constant as the traverse range is increased. Corner reflections as possible explanations can be ruled out by similar considerations.

There remain two feasible sources of interference -- the hydrophone end-wall reflection and modes of a higher order. As the traverse range is increased by an increment λ in moving the hydrophone toward the hydrophone end wall, the path length of the end-wall reflection is decreased by the same increment. It can be seen then that interference peaks with the observed spacing would arise from such variations in path lengths. Furthermore the amplitude of the interference would increase as the transverse range increases. Amplitude-wise the problem is more difficult and will be discussed in section 3.2.3. It will suffice here to say that the amplitude of the end-wall reflection observed in pulse experiments does not appear to be sufficiently large to provide the pattern discussed above. It may be, however, that with a continuous-wave signal the standing wave produced by this reflection builds up to sufficient amplitude.

That the interference is caused by the re-radiation of bottom-propagated energy has been considered highly improbable. There exists no evidence for bottom waves with wave lengths of the value necessary to provide the observed spacing of the interference peaks. Rather it is more likely that one or more modes of order number greater than four are contributing significantly to the sound field. In both the rigid bottom and fluid bottom calculation of the sound field for the conditions H/2=h=d, four normal modes were propagating. Higher order modes appeared highly damped. It is possible that one or more of the latter modes is not as highly damped in the ranges used in the experiment as was presumed. Such a mechanism has the advantage of explaining also the apparent decrease in amplitude of interferences with range in the measurements at other than mid-depth. Computations and measurements are in progress to attempt to determine the effects on the sound field of various degrees of attenuation of these higher order modes and to examine their depth dependence. It has been shown, as will be discussed in a later section, that the pulse signals lose little energy per bottom reflection. This fact enhances the possibility that the higher order modes may not be as highly attenuated as was first believed.

Frequencies below 4 Kcps -- In order to gain added knowledge of the acoustic properties of the bottom of the tanks a number of experiments have been carried out to measure the frequencies at which the various normal modes "cut-on" or being to propagate. It was intended to make a comparison of the measured cut-on frequencies with those calculated assuming each of the various bottom conditions.

As shown in the preceding theoretical sections for a constant water depth and bottom condition there is a critical frequency for every normal mode below which a given mode will be attenuated. The nature and degree of dependence of these frequencies upon the depths of the layers of the bottom media and upon certain of the physical constants of these media have been calculated and observed heretofore with considerable agreement in some of the less complex situations.

In a specified, constant experimental situation one might expect to be able to observe the onset (rapid decrease of attenuation) of at least a few of the modes of lower order number by observing the change in amplitude of the field with range as the frequency is increased. From theoretical considerations one would anticipate a linear relation between the logarithm of the amplitude and the range after accounting for cylindrical spreading for frequencies below cut-on of the zeroth order mode. When this mode is fully propagating the curve should remain straight, and upon being corrected for cylindrical spreading should approach a constant average amplitude as a function of range (barring other sources of attenuation). Such change represents the increase of energy propagated by the now non-damped zeroth order mode.

Cut-on of the first order mode should give a regular periodicity to the amplitude of the field at a higher mean amplitude level. The advent of each of the higher order modes results in a more complex amplitude variation at still higher mean levels. The values of the mean amplitudes with various numbers of modes propagating, the periodicities, and the frequencies at which these changes occur are related to the layer depths and physical constants of the media involved as discussed in earlier sections.

In Table II are the calculated cut-on frequencies of the various orders (n) of modes for each of three postulated bottom types. Values of

the physical constants used are the best presently available for the materials in the concrete tank. Values of c_1, b, and H are undoubtedly reliable. The values given for c_c and c_s are those derived by methods discussed in section 3.2.3 of this report concerning one-millisecond pulse experiments. The formulae for cut-on frequencies may be derived directly from the period equations developed in section 3.1.2. These formulae are given below.

$$f_n = \omega_n/2\pi$$

For rigid bottom:

$$\omega_n = \frac{c_1(2n+1)\pi}{2H}$$

For fluid bottom:

$$\omega_n = \frac{c_c}{\sqrt{\frac{c_c^2}{c_1^2} - 1}} \quad \frac{(2n+1)\pi}{2H}$$

For elastic bottom:

$$\omega_n = \frac{c_s}{H\sqrt{\frac{c_s^2}{c_1^2} - 1}} \left[pp \tan^{-1} \left(- \frac{1}{b} \frac{c_c}{c_s} \frac{\sqrt{\frac{c_s^2}{c_1^2} - 1}}{\sqrt{\frac{c_c^2}{c_1^2} - 1}} \right) + n\pi \right]$$

Explanation and values of symbols used in Tables II and III:

ω (angular frequency in radians per second)

f (acoustic frequency in cycles per second)

n (mode order number)

pp (principal part)

c_1 = 4800 ft/sec (velocity of sound in water)

c_c (velocity of compressional wave in concrete bottom)

c_s (velocity of shear wave in concrete bottom)

b = 0.43 (ratio of water density to concrete density)

H = 2.37 ft (water depth)

TABLE II

Calculated cut-on frequencies f_n for different types of bottom. c_c = 12,300 ft/sec, c_s = 7,070 ft/sec.

Bottom type	n	ω_n	f_n
Rigid	0	1013π rad/sec	507 cps
	1	3040π	1520
	2	5080π	2540
	3	7100π	3550
	4	9120π	4560
Fluid	0	1080π	540
	1	3250π	1625
	2	5400π	2700
	3	7580π	3790
	4	9740π	4870
Elastic	0	1800π	900
	1	4520π	2260
	2	7260π	3630
	3	$10,000\pi$	5000
	4	$12,800\pi$	6400

TABLE III

Calculated cut-on frequencies f_n for different types of bottom. c_c = 16,250 ft/sec, c_s = 8,960 ft/sec.

Bottom type	n	ω_n	f_n
Rigid	0	1013π rad/sec	507 cps
	1	3040π	1520
	2	5080π	2540
	3	7100π	3550
Fluid	0	1064π	532
	1	3192π	1596
	2	5320π	2660
	3	7448π	3724
Elastic	0	1550π	775
	1	3960π	1980
	2	6375π	3188
	3	8780π	4390

In the experiments conducted for the purpose of observing the amplitude behavior as a function of frequency, conditions were set such that $h = d = H/2 = \lambda$ for a frequency of 4 kcps. The frequency was varied thereafter and amplitude measurements were made as a function of range. One set of data

was taken using 8 millisecond pulses and suitable band pass filters. There was essential agreement between this and the c-w data.

Figures 24 and 25 show some of the c-w measurements with cylindrical spreading removed. For this experiment the voltage at the projector (1K) was adjusted at each frequency to produce identical hydrophone outputs at a range of 1 foot. This procedure obscures the observation of mean pressure amplitude increment increases as modes above the zeroth order mode cut-on. To deduce this type of information from the data one must introduce corrections for projector output variations with frequency (which are available only for a free field situation) which implies knowledge of the effect of the experimental parameters on the impedance of the projector. The impedance was not measured.

However, several factors of interest are available from the data of Figs. 24 and 25. Below 700 cps the field is highly damped and the amplitudes in db fall off in range almost linearly. In this frequency region, which is apparently below cut-on of the zeroth order mode, there are slight incremental decreases in attenuation with each increment increase in frequency. The curves are not straight lines, but are somewhat concave upward with definite indications of a major decrease in rate of fall off beyond a range of 6.5 - 7.5 ft. The concavity and the "elbow" at the range of about 7 ft may be attributed to the higher attenuation of the higher modes. The incremental rises in amplitude with frequency are probably caused by the approach to zeroth order mode cut-on. The apparently anomalous behavior of the 400 cps curve is believed to be a result of the beginning of a deterioration from a sine wave of the projected wave form at this frequency, a phenomenon that progressively worsens at still lower frequencies.

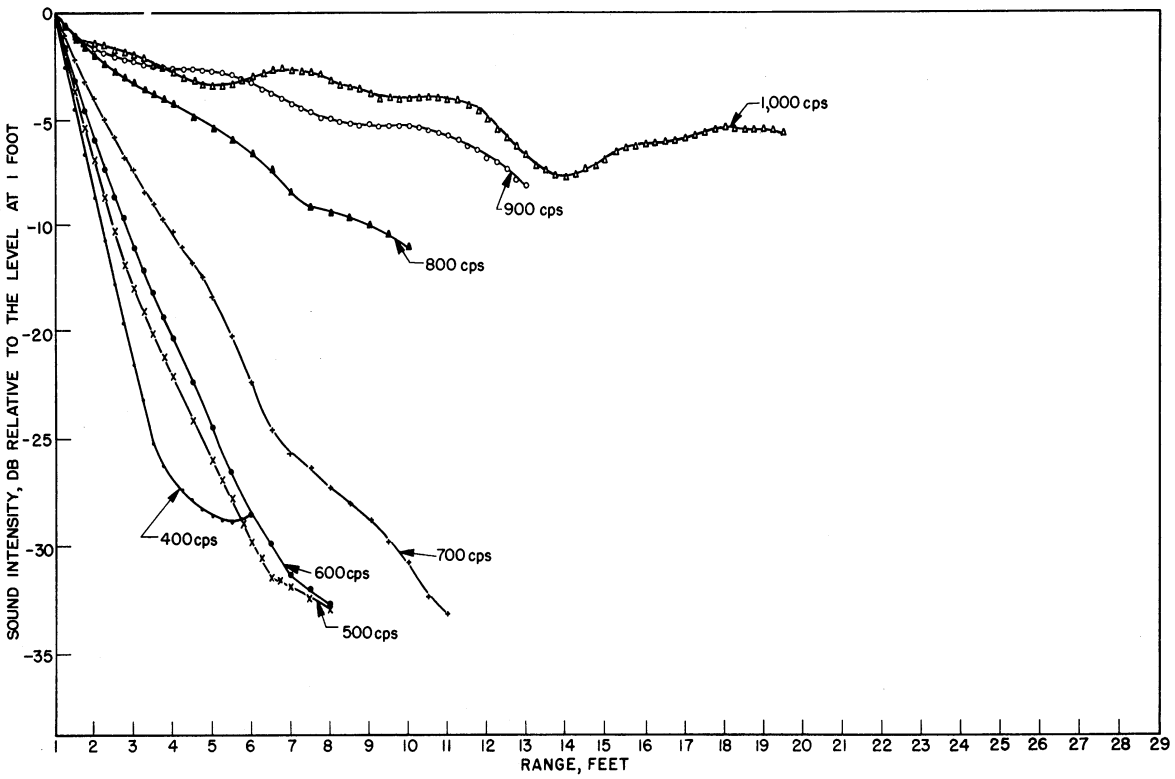

Fig. 24. Measured sound intensity variation with range at different frequencies. $H/2 = h = d = \lambda(4\text{kcps})$. The correction for cylindrical spreading has been made.

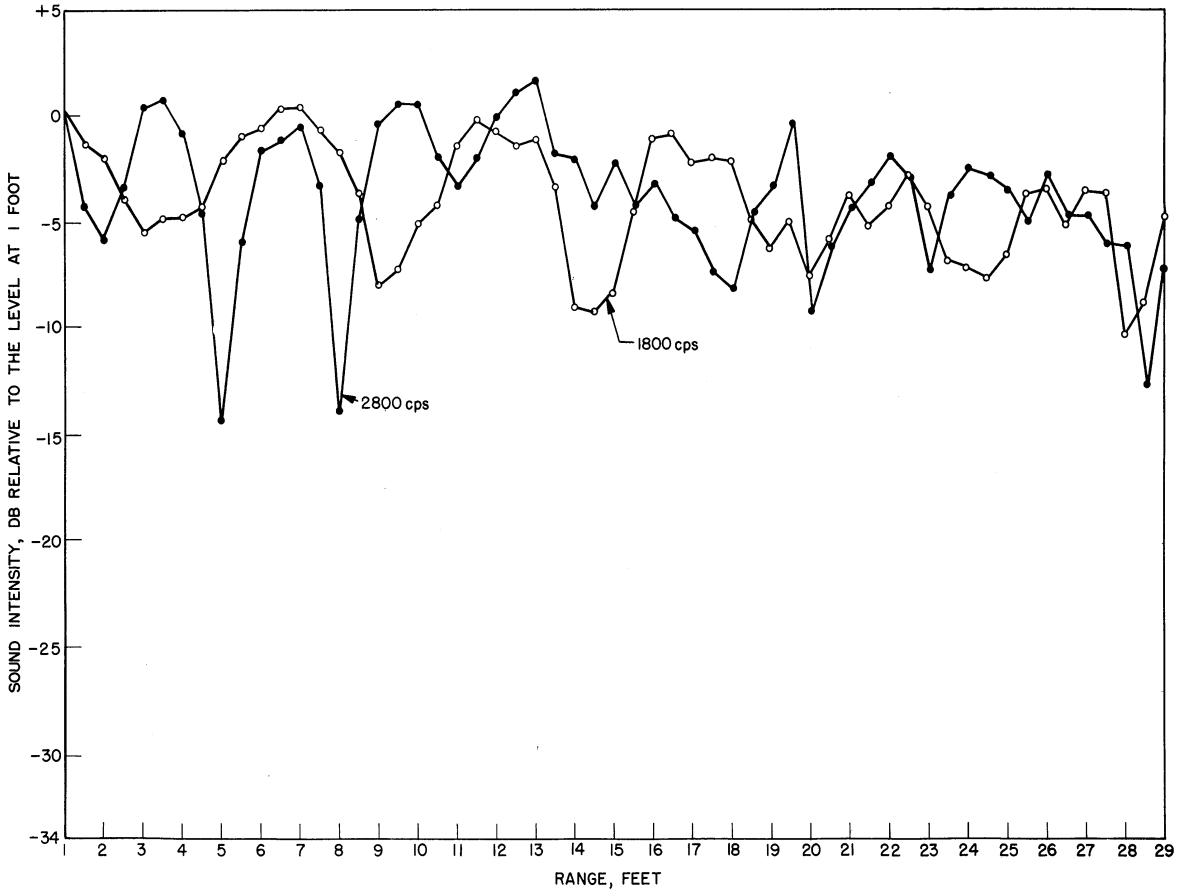

Fig. 25. Continuation of Fig. 24.

Between 600 and 1000 cps it appears that the zeroth order mode becomes fully propagating. The data show rapid decreases of attenuation as a function of frequency with the major jump occurring between 700 and 800 cps. From these data it would appear that the mode cuts on relatively slowly with increasing frequency and that indeed it does not become fully propagating until a frequency of 900 or 1000 cps is attained. This is to be compared with predicted cut-on frequencies of 507, 540 and 900 cps for rigid, fluid, and elastic bottoms, respectively using tank experimental values for velocities in the bottom. Substitution of Shell Exploration and Production Company values for bottom velocities in wet concrete yields analogous cut-on frequencies of 507, 532, and 775 cps.

In Fig. 25 amplitude data for the frequencies of 1800 and 2800 cps are shown. It is fairly evident that at both frequencies the spacing of maxima and minima of the amplitude is uniform with smaller spacings at the higher frequency. This trend is further exemplified by a still shorter spacing at 3300 cps as revealed in the corresponding 8 ms pulse data. Ideally the trend is predictable, and the exact spacing is also predictable if the proper longitudinal and shear wave velocities and the density of the bottom are known.

The problem is to compute the difference in range between two points in the periodic variation of the field which are one cycle apart. If one chooses a frequency at which two normal modes should be propagating, the real part of the field of each of the modes can be represented by the form $A_0\sin(k_0 r-\omega t)$ and $A_1\sin(k_1 r-\omega t)$ respectively (for modes of order numbers 0 and 1). Here A is the amplitude, r the distance from the source, ω the angular frequency, t the time, and k_0 and k_1 the k numbers associated with each mode (see section 3.1.1). Constructive interference between modes will occur where the two modes are in phase or at range r_1 where

$$k_0 r_1 - k_1 r_1 = 2n\pi \qquad n = \text{integer}$$

and at range r_2 where

$$k_0 r_2 - k_1 r_2 = 2(n+1)\pi \ .$$

From the above equations one finds the desired spacing

$$r_2 - r_1 = \Delta r = \frac{2\pi}{k_0 - k_1} \ . \qquad (1)$$

The frequency chosen for comparison was 2800 cps. At this frequency if one assumes an elastic bottom and uses the Shell Exploration and Production Company bottom velocity values, two propagating modes are predicted. The spacing between maxima produced by these two modes can be computed as above. The two-mode spacing has been calculated for this condition.

For the calculation of the spacing considering an elastic bottom an iteration process must be employed to operate on the period equation and thus arrive at values for the k numbers involved. The period equation as derived in section 3.1.1 is given below.

$$\tan x = \frac{x}{bH}\left[4\sqrt{\frac{\omega^2}{c_1^2} - \frac{\omega^2}{c_s^2} - \frac{x^2}{H^2}}\ \frac{\left(\frac{\omega^2}{c_1^2} - \frac{x^2}{H^2}\right) - \left\{1 - 2\left(\frac{\omega^2}{c_1^2} - x^2 H^2\right)\right\}^2}{k_s^4 \sqrt{\frac{\omega^2}{c_1^2} - \frac{\omega^2}{c_c^2} - \frac{x^2}{H^2}}}\right]$$

The meanings of the above symbols are:

c_1 = 4,800 ft/sec (velocity of sound in water)

c_s = 8,960 ft/sec (velocity of shear wave in concrete)

c_c = 16,250 ft/sec (velocity of compressional wave in concrete)

H = 2.37 ft (water depth)

b = 0.435 (ratio of density of water to that of concrete)

ω = 2π x frequency = $2\pi(2800)$

$$\tan x = 0.982x \left[\sqrt{k_n^2 - 3.86}\ (.268\ k_n^2) - \frac{(1 - 0.518\ k_n^2)^2}{\sqrt{k_n^2 - 1.17}} \right]$$

where $k_n^2 = k^2 - (n+1/2)^2(\pi/H)^2$

and $k^2 = \omega^2/c_1^2$

By iteration the k_n's are obtained.

$k_0 = 2.20$ for x = 6.94 radians

$k_1 = 3.15$ for x = 4.42 radians

From Eq. (1)

$$\Delta r_{0,1} = 6.6 \text{ ft}$$

From the measurements of amplitude versus range in the tank at 2800 cps one obtains a spacing of 3 feet. Obviously this is not in agreement with the value computed above in the elastic-bottom two-mode calculation. The reason for this behavior is unknown. A combination of a low amplitude for one of the two propagating modes at mid-depth and a beginning of the third mode cut-on (predicted at 3188 cps) might possibly result in such a spacing. Both experimental and theoretical effort on the possible contributions of modal amplitude depth dependence, branch line integrals, and highly damped modes at this frequency are high in priority for future work.

Another factor to be noted in the figures is the increasing "fine structure" of the amplitudes with increasing range. This is similar to the interference noted previously at 4000 cps.

3.2.3. Pulse Experiments

Considerable effort was expended in experiments using short pulse signals both at 10 kcps and 4 kcps for conditions where $h = d = H/2 = \lambda$. The possible value of the short pulse experiments, it was believed, was two-fold. First it was expected that data could be obtained at least over a portion of the range free from wall-reflection interference. Secondly, one should be able to get a direct measure of the amplitude of the wall reflection relative to the direct field. With the closest walls to the range line in the two tanks being 20 feet and 26.5 feet respectively, one expects no interference with the direct path signal from reflections from these walls using a 1 ms pulse over the entire range used in the experimental work. With a 4 ms pulse this range of non-interference of side-wall reflections with the direct pulse would be limited to about 30 feet in the narrower tank. If one considers elongation or distortion of the received signal due to image effect or mode group velocity differences then this non-interference range becomes somewhat shorter.

Wall Reflections - Experiments designed to examine the amplitudes of side-wall reflections have been carried out at 4 and 10 kcps in various depths of water. At each depth where both frequencies were employed all experimental conditions were identical except for pulse lengths. The projector and receiver hydrophone were at mid-depth in all cases. Ideally, it would have been desirable to use 1 ms pulses in all cases. However at 10 kcps only 2 ms tape-recorded pulses were available. Table IV lists the water depths used, frequencies, pulse lengths, and ratios at ranges of 20 feet of the amplitude of the direct water path signal to that of the side-wall reflection wherever the latter was observed.

TABLE IV
Ratios of amplitudes of direct signal to side-wall reflection for pulses at 4 and 10 kcps and various depths

Water depth	4 kcps		10 kcps	
	Pulse length	Amplitude ratio at range=20 ft Direct:Reflected	Pulse length	Amplitude ratio at range=20 ft Direct:Reflected
0.95 ft	1 ms	no reflection observed	2 ms	6:1
2.36	1	" " "		
2.86	1	" " "		
3.00	1	" " "		
3.70	1	3:1	2	1:1

It should be noted that $H = 0.95$ ft $= 2\lambda$ at 10 kcps and $H = 2.36$ ft $= 2\lambda$ at 4 kcps. Under these conditions and the assumption of a rigid bottom it has been calculated that 4 normal modes should propagate. Also when the direct path range is 20 ft the path length for the side-wall reflection is 44.6 ft.

It is seen above that there are no discernable side-wall reflections at 4 kcps except at the deepest water depth. Here at the range of 20 ft the wall-reflected signal is superimposed upon the higher order top- and bottom-reflected pulses which are of comparable amplitude. Acknowledging the difficulty of amplitude measurement imposed by the presence of top- and bottom-reflected pulses superimposed on the side-wall reflections it appears that the ratio of the direct path signal amplitude to that of the wall reflection is of the order of 3:1 at this deepest depth.

On the other hand it is to be noted that for 10 kcps there is clear evidence for the wall reflections at both the shallow and deep depths. The estimated ratios of direct to wall-reflected signal amplitudes are 6:1 and 1:1 respectively at a 20 foot range.

Over the traverse ranges employed the path length of the side-wall reflections in the tank of greatest width (where most of the c-w data was obtained) varied between 50 and 75 feet. The path length for the hydrophone end-wall reflection varies between 75 and 130 ft. Some time was spent in pulse experiments searching out the end-wall reflection. Positive identification was made by correlating times of arrival of the reflected pulse with changes of range of the hydrophone.

Since all the effort at the time these measurements were made was in pulse work, this reflection was deemed a negligible influence on the field for two reasons. Its amplitude was very small, and its arrival time was such that the reflection did not interfere with the received signal over most of the ranges being worked. The later appearance of interference peaks in c-w experiments at range increments of approximately $\lambda/2$ indicates that at the long traverse ranges where one is working relatively close to the end wall and the reflected signal amplitude becomes more nearly comparable to that of the direct signal, such interferences may be the result.

In order to give a plausible interpretation to these observations, several other facts believed to be pertinent are described in the following paragraphs.

To date almost all ranges employed in both the c-w and pulse experiments have been of the order of 20 - 35 ft. It has been noted in section 3.2.2 "Continuous-Wave Experiments" that essentially good agreement between the c-w pressure amplitude measurements and the rigid bottom calculation has been obtained. These c-w measurements and those made in the mode cut-on experiments both show an increase in "structure" at the longer ranges measured.

In a subsequent section 3.2.2 "One Millisecond Pulse Experiments" there is a discussion of the separation in time of source image reflected pulses and of the measurements of their individual amplitudes as a function

of range and incident angle. It will suffice at this point to say that the measurements provide no observable loss on reflection at the bottom. In addition there is a small peak in the amplitudes of each of these source image reflections at an incident angle of approximately 23°. The data further suggest that this phenomenon is followed by a slight decrease in amplitude and a subsequent rise as the incident angles increase. These effects are quite small and are observed as slight perturbations on the reflected pulse amplitude range curves which seem otherwise to conform within experimental error to the spherical spreading law. At these ranges and available water depths, it is certainly questionable as to whether measurements are being made in the far field. That is, the data taken may be indicative of intermediate ranges wherein certain pertinent phenomena are occurring. These phenomena include the possibility of a spherical wave-front, which would influence phase considerations and reflection coefficients; also the change in incident angle for the various source image rays from 0° to angles beyond those critical for cut-off of compressional and shear wave propagation in the bottom does not ordinarily occur in the far field.

Any valid hypothesis regarding the nature of the propagation in the tanks must satisfactorily reconcile the observations mentioned above. These are summarized as follows --

1. Wall reflections decrease (with respect to direct signal) with decrease in water depth and with increase in frequency at a given range.
2. Over the limited range considered the measured field agrees moderately with the rigid bottom calculation.
3. The source image amplitude range dependence indicates a high bottom reflection coefficient at all angles of incidence.
4. The source image amplitudes possess a small peak at an angle of incidence of 23°, and then a slight fall off and subsequent recovery as the incident angle is increased.

Effect of Variations in Pulse Length - In section 3.1.2 calculations are made to show the time dependence of the pulse shapes for the normal mode approximation and for the summation of the image series with a rigid bottom assumption. For a 3 ms pulse ($H/2 = \lambda = d = h = 1$ ft) it can be seen that in only a fraction of the received signal are the four normal modes in time coincidence because of the different group velocities of the modes. That is, one would be compelled to be extremely careful in observing the received signal in order to measure the amplitude corresponding to the vector addition of four modes. Experience with this experimental arrangement in the model has demonstrated that one must go to pulse lengths on the order of 6 to 8 ms in order to obtain a field which corresponds with the c-w field at the ranges used here; the pulse length must be longer for larger ranges. Figure 26 shows the results of range runs ($H/2 = \lambda = d = h = 1$ ft) using 4, 6, and 8 ms pulses. Only the 8 ms pulse length provides a field which corresponds closely with the c-w field and, with the exception again of the additional measured peak at 26 feet range, corresponds with the rigid bottom calculations.

The shape of 1 ms pulses in the tanks is qualitatively similar to that predicted in section 3.1.2 and shown in Fig. 18. Experiments with various values of H and with several values of h and d have been performed. The records from these clearly demonstrate the arrivals of the pulses reflected from the water surface and the bottom and extending to very high order reflections. Greater values of H serve to separate clearly the individual reflected pulses. A more complete discussion of the 1 ms pulse data is given later in this section.

No attempt has been made thus far to achieve detailed agreement between experimental pulse shape and that predicted. It is hoped that in the future the pulse shape may be studied in more detail. To date the prime

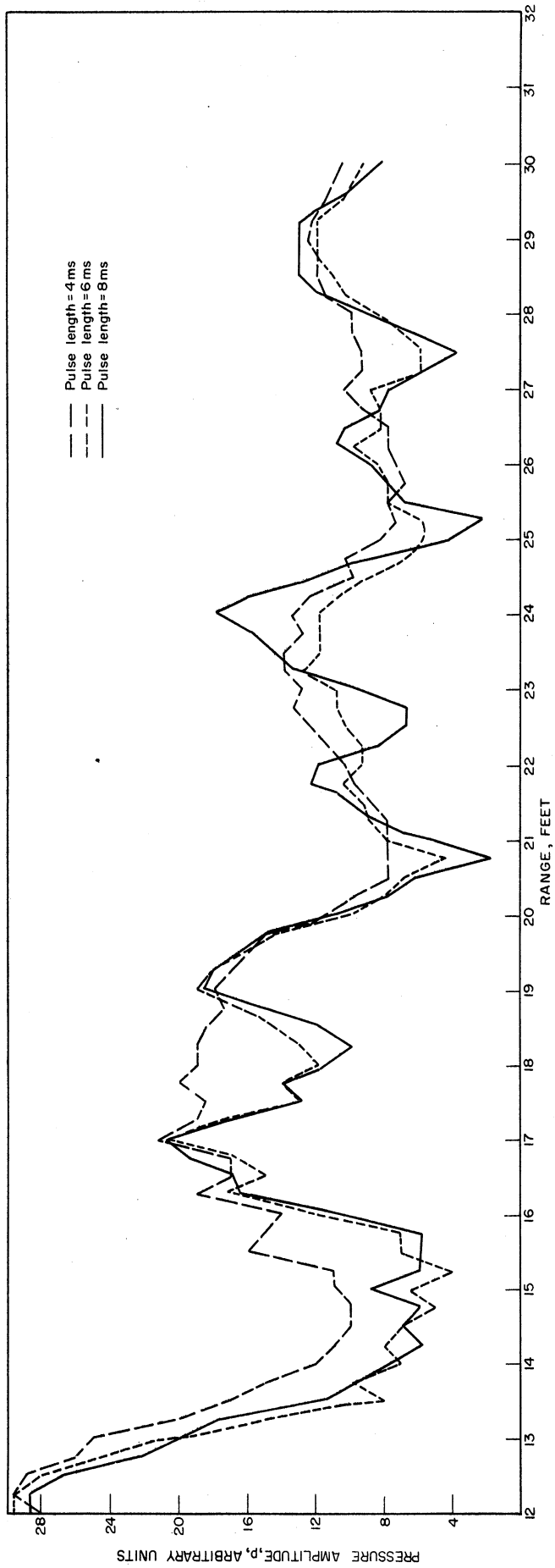

Fig. 26. Measured pressure amplitude variation with range for different pulse lengths. Frequency = 4 kcps, $H/2 = h = d = \lambda$.

purpose for varying the pulse length has been to attempt to observe the field in the absence of wall reflections, although this is not to minimize the value of other information gained in connection with the pulse experiments.

One Millisecond-Pulse Experiments - It had been planned at the outset of the tank work to investigate the behavior of very short pulse lengths. It was believed that it might be particularly interesting if the cycles in the pulse could be readily discernable in order to examine interferences in detail. The image-like appearance of the received signal in the instances of the shorter pulse-length experiments indicated that a considerable amount of information might be obtained through the use of even shorter pulse lengths. A number of features which one might wish to examine by these means are:

a. top and bottom reflections,

b. wall reflections,

c. normal mode build-up mechanism,

d. bottom transmitted energy.

Various experiments have been run using one ms pulses. The main parameter varied was H, the water depth. Other factors that were varied were h and d, (receiver and projector depths), and the position of the range. The experiments were run in both of the two available tanks. The first tank used allows a maximum water depth eight inches greater than the second and possesses more cracks in the bottom. The significance of the cracks is clarified in later paragraphs "Study of Bottom Characteristics".

A loop of magnetic tape was made on which several one-millisecond 4 kcps pulses were recorded. The transmitted signals were examined and their shape at very short ranges was quite similar to that of the pulses recorded on the magnetic tape. The x-axis of the oscilloscope was expanded so that the four cycles of 4 kcps pulse were clearly separated.

Figure 27 is a representative plot of data taken when H = 3 ft and h = d = 1.5 ft. The range was along the center-line of the tank parallel

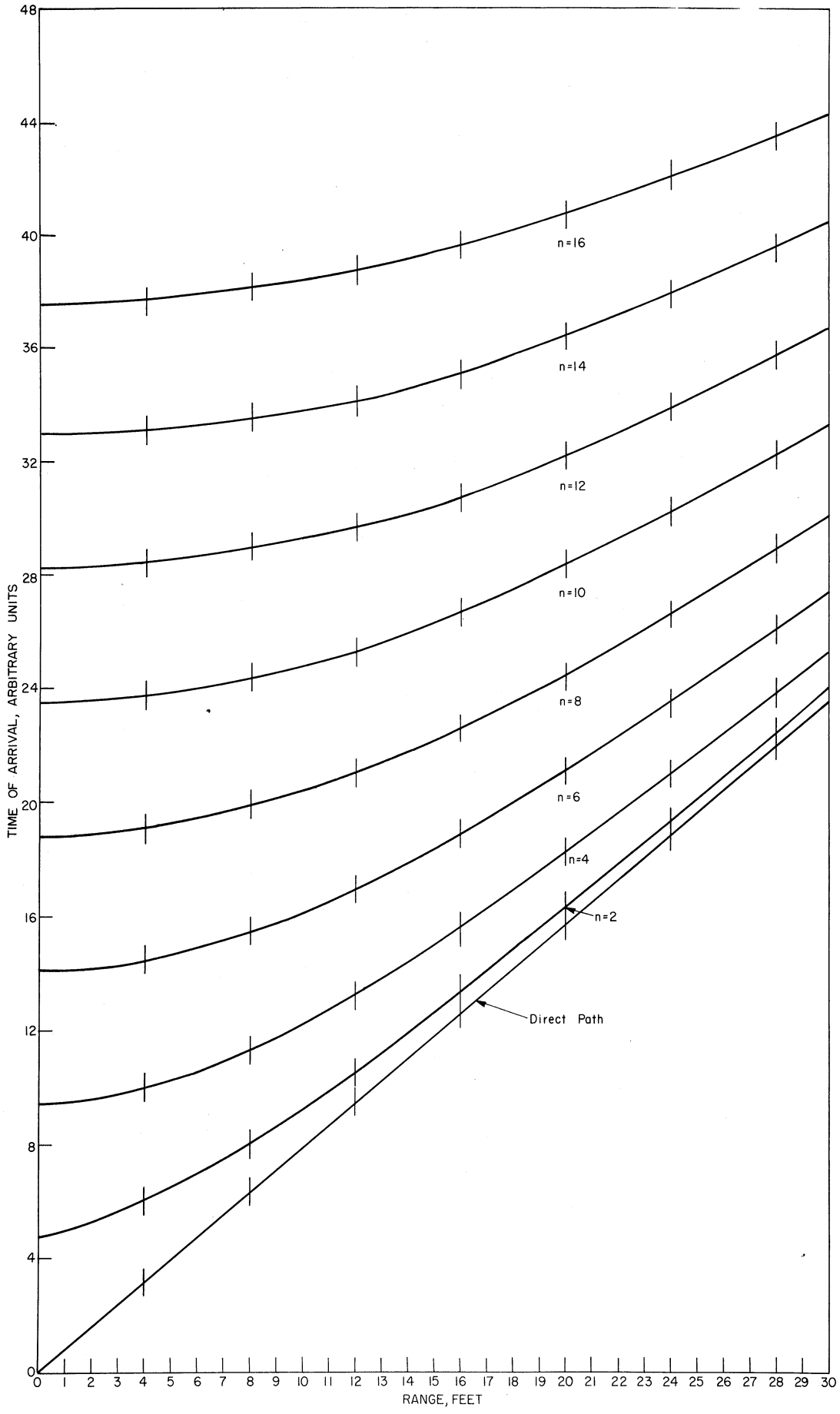

Fig. 27. Calculated variation of arrival time with range for several even numbered top- and bottom-reflections and the direct path signal. Pulse length = 1 ms, frequency = 4 kcps, H/2 = h = d = 1.5 ft. Length of vertical bars indicates spread of data.

to the longer (side) walls and midway between the shorter (end) walls. The curves are the calculated times of arrival (TA) of the various even-numbered top and bottom reflections at the ranges shown. For example, $n = 4$ is the case where the reflected signal had experienced two top and two bottom reflections. (See Fig. 28.) It is apparent from the small signal size that the 180° phase shift occurring at the surface reflection and, incidentally, the lack of significant phase shifting at the bottom, eliminated odd-numbered arrivals. This means, of course, that effectively the odd-numbered reflections of equal path length are phased out.

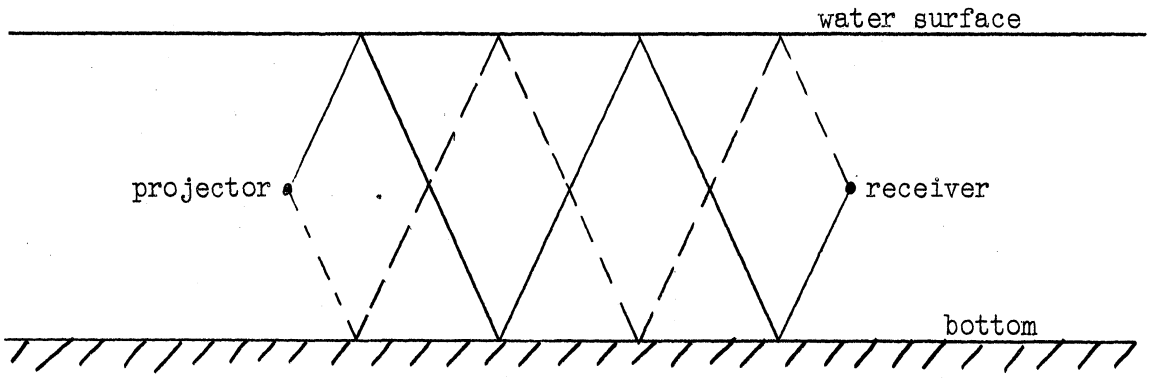

Fig. 28. Ray diagram for sound paths where $n = 4$ (2 top and 2 bottom reflections).

Most of the spread in the data (length of the vertical bars) can be attributed to the method of reading the pulses. Times were measured on the oscilloscope photographs from the sweep start to the peaks of the highest amplitude positive half-cycle and highest amplitude negative half-cycle in each pulse at each range. This procedure results in at least a half-cycle to a whole-cycle spread in the data. Very slight variations in the start of the oscilloscope sweep also contributed slight errors. The curves on the plot represent the TA's of the pulse "centers" minus a time corresponding

to one-half the pulse length. The length of the vertical bars represents the spread of the measured time of arrivals; the bars are arbitrarily spaced on the graph at 16 times the measuring range intervals.

With the velocity of sound in water constant, the change in path length with increasing image order number is a function of the water depth and range. For a given pulse length and over the ranges here considered there exists a minimum depth at which the received signals of consecutive order images just fail to overlap each other in time. As the depth is increased beyond this minimum the signals separate further in time. In a deeper water experiment the separation of the pulses is more readily discerned. This fact results in clearer observation of reflected pulse arrival times and amplitudes.

With the projector and receiver not at mid-depth the path lengths for the odd-order reflections are no longer equal. In an experiment where $H = 3.7$ ft and $h = d = 0.84$ ft one can note the effect just mentioned. The phase shift between top and bottom reflected odd-order images is no longer 180° due to the path length differences, and signals of significant amplitudes are introduced. (See below.)

Figures 29 and 30 show photographs of the oscilloscope screen taken at hydrophone ranges of 1 foot and 17 feet, respectively. At one foot there are few reflected pulses. The wall reflection appears toward the right end of the sweep. At a range of 17 feet several even-numbered reflections can be seen. Gain increases between two and 17 feet have been made as the direct pulse decreased in amplitude in order to observe the detail in the reflected pulses.

In comparing a plot of the measured times of arrival with the calculated times it is seen that when the projector and hydrophone are not at mid-depth the odd-numbered reflections are not cancelled by phase shifts.

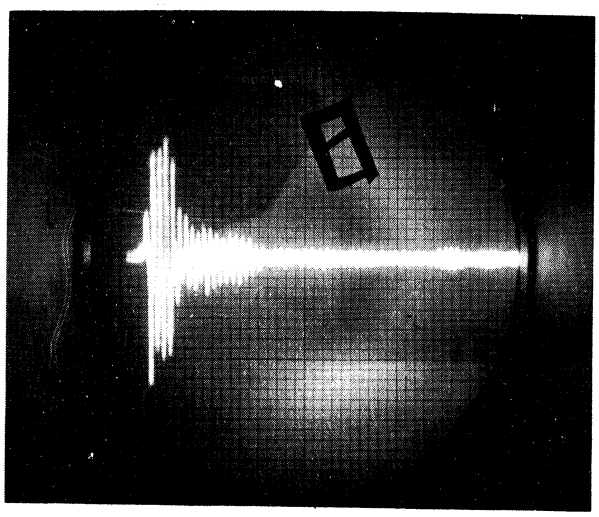

Fig. 29. Photograph of oscilloscope screen showing received signal at a range of 1 foot. Pulse length = 1 ms, frequency = 4 kcps, H = 3.7 ft, h = d = 0.84 ft.

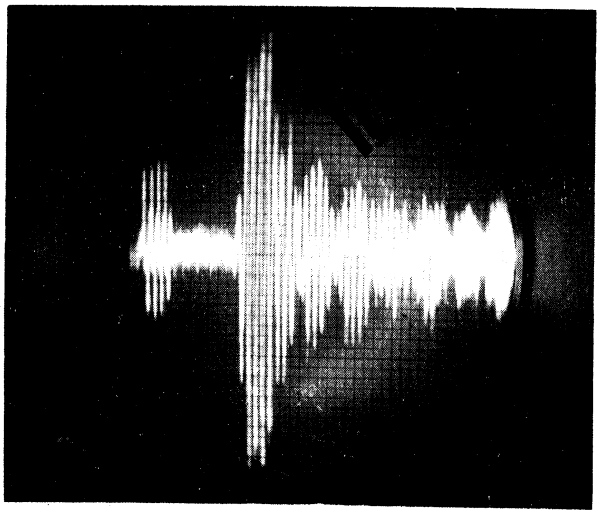

Fig. 30. Photograph of oscilloscope screen showing received signal at a range of 17 ft. Pulse length = 1 ms, frequency = 4 kcps, H = 3.7 ft, h = d = 0.84 ft.

The calculation shows a group of families of curves, each family consisting of three closely spaced curves. The transmission paths which yield these curves are shown in Fig. 31. If, in a given family, the center curve is for an even-numbered reflection time of arrival n, then immediately below it is the curve for $(n-1)_D$. The subscript D indicates that the reflected pulse left the projector in a downward direction. Similarly, immediately above the n curve is the curve for $(n+1)_U$ where the subscript U indicates the reflected pulse left the projector in an upward direction. The comparatively small differences in path length between these three reflected pulses account for the grouping into a "family". The spread of the plotted data shows the broadening resulting from this phenomenon. The shapes of the calculated and measured curves are identical except for a slight error due to the non-linearity of the oscilloscope sweep.

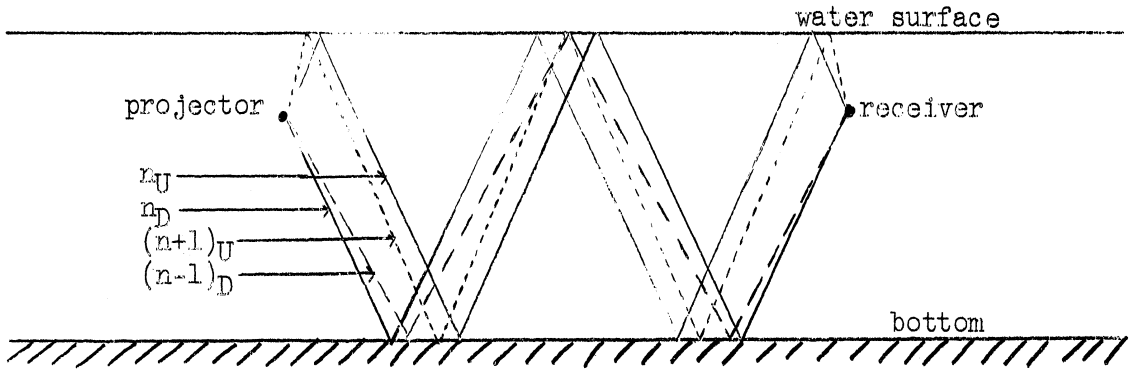

Fig. 31. Ray diagram for sound paths where $n_U = n_D = 4$, $(n+1)_U = 5$, $(n-1)_D = 3$.

Referring again to Fig. 30 the appearance of reflected pulses at the longer range suggests an investigation of the amplitudes of the reflected pulses as a function of range. The pressure amplitude of each of the even-numbered reflections was measured, corrected for spherical spreading, and plotted as a function of range. Such a plot for $n = 4$ is given in Fig. 32. Here one might expect, as predicted in section 3.1.2 of this report, to find an indication of the range at which the critical angle of reflection for $n = 4$ is exceeded. The rise in pressure amplitude giving evidence of a peak at a range of 6 feet is interpreted as an indication of such a cut-on. As is shown in the figure the critical angle calculated for this cut-on is 22°. This may be interpreted as the critical angle for the compressional wave in the concrete. Likewise predicted by section 3.1.2 of this report is a cut-on or critical angle for the shear wave propagated in the bottom. The experimental evidence, though very tenuous, suggests that the critical angle for shear wave is approximately 43°.

Similar plots for higher orders lend further credence to this interpretation. The mean measured compressional wave critical angle for six different orders of even-numbered reflections is 23°27' with a maximum deviation from the mean of 1°24". In the same range of n's only two vague suggestions of shear wave critical angle can be found giving angles of 42°33' and 42°55'. These critical angles yield compressional and shear wave velocities in the bottom of 12,280 ft/sec and 7,070 ft/sec, respectively. The characteristics of the bottom are discussed later in the report. These values of velocities, it should be noted, are reasonable for concrete.

The probability for the data to yield such consistent values of the compressional wave velocity by chance is computed to be less than 1:370. This ratio was calculated as follows. Seven different even-ordered reflected pulse amplitude vs range curves were measureable ($n = 2$ through $n = 14$). Two

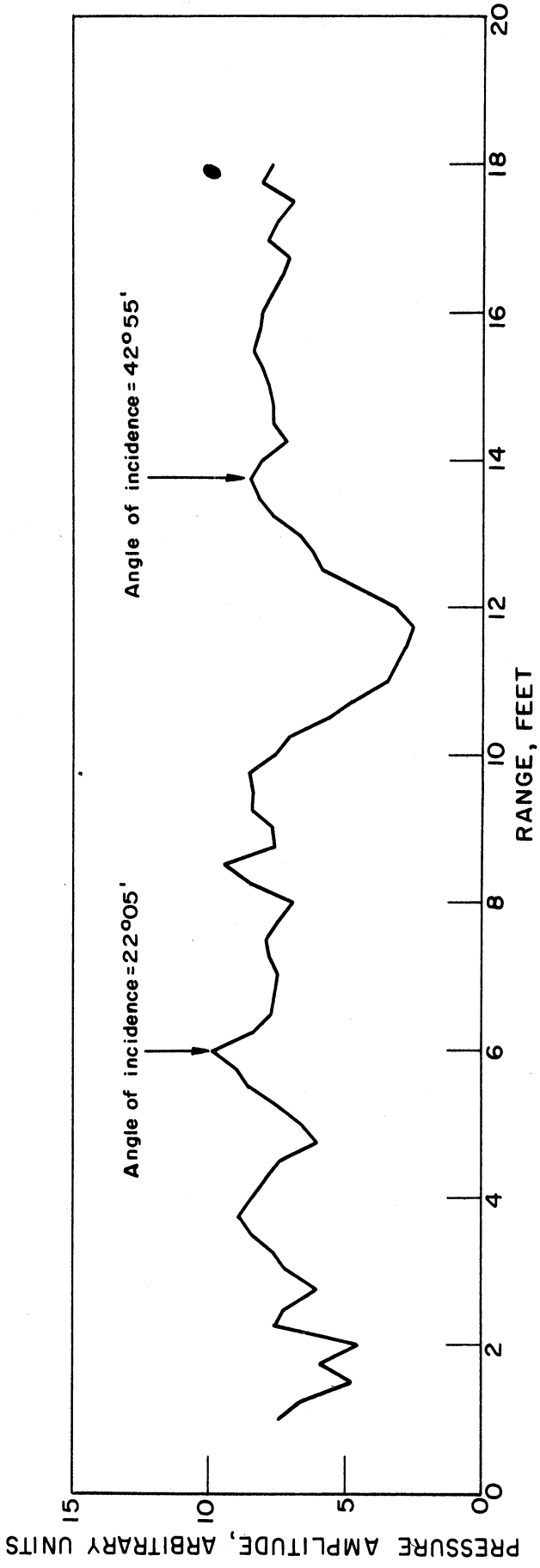

Fig. 32. Measured pressure amplitude variation with range of 1 ms, 4 kcps pulse for n = 4 (2 top and 2 bottom reflections).

of the seven did not meet the acceptance criterion which was that after correction of the amplitudes for spherical spreading, the highest amplitude peak on each plot must fall within the total spread in angle of 2.5° centered on the critical angle. The average range of incident angles over which the amplitudes of the various orders of reflection were measured was about 15°. One of the two rejected measurements gave a clear peak at 24°31' but a higher one existed at 28°. The second rejection gave peaks at 18° and 26° but at a range where the reflected pulse and direct water path signal interfered.

The above data are not consistent with the velocity information from the Shell Exploration and Production Company. The latter results give compressional wave velocities of 15,350 ft/sec and 16,250 ft/sec for dry and wet concrete and shear wave velocities of 9,160 ft/sec and 8,960 ft/sec respectively for dry and wet samples. Using the same value for the velocity of sound in water (4800 ft/sec) and the Shell wet concrete velocity values, the calculated values of compressional and shear wave critical angles are 17°27' and 28°33'.

The reason for the lack of agreement is not clear. Weinstein[5] has observed experimental variations in the value of the reflection coefficient from that predicted by plane wave theory when the angle of incidence is such that the change of phase upon reflection varies greatly with a small change in the angle of incidence. In these regions especially one cannot use a divergent beam several degrees wide to approximate at a plane wave. Weinstein demonstrates a shift of the reflection peak at the critical angle for the compressional wave and a major minimum in the reflection amplitude in the region near the critical angle for shear. He uses a thick aluminum plate as a semi-infinite reflector. These observations are qualitatively similar to some of the reflection data taken in the tanks. Further experimental effort is indicated.

It is possible that theoretical work now in progress will determine the correction factor needed to convert reflection coefficients obtained with

spherical waves to the plane wave coefficients. Another possibility is that the introduction of a damping factor due to shear wave attenuation may clear up the inconsistency.

Attention is now turned to the consideration of bottom-propagated energy. Exhaustive search for evidence of this energy at the working frequencies (4 and 10 kcps) have been made in tank number one. The net result was that there was only slight evidence for some low-level bottom-transmitted energy. It was concluded that a better approach would probably be to investigate this phenomenon by means of an impulse source. However, since the signal at these frequencies was so weak that it was believed of little significance to the amplitude measurements, and the impulse-type of experiment was deferred. It is evident that joints and cracks in the bottom of the tank will strongly influence bottom propagated energy. These effects will be discussed in a later section.

After the experiment was moved to the second tank and more runs were made with one millisecond pulses, any existing doubt about the presence of bottom propagated energy was removed. The photograph shown in Fig. 33 clearly shows a low amplitude early arrival. It should be pointed out that the data from which this photograph was selected were not taken for the express purpose of investigating bottom-transmitted energy. It is felt that these experiments can be improved in the future.

The above-mentioned data give an apparent bottom-propagated wave which preceeds the direct water-propagated wave at a range roughly determined to be between 5.5 and 6.5 feet. The uncertainties of the experiment do not allow one to compute exactly from the data the velocity of this bottom wave. Calculations reveal, however, that the measured range spread given above is close enough to the calculated range of the first arrival preceding the water propagated wave so that a presumed shear or Rayleigh wave velocity of the order of 7000 - 9000 ft/sec could account for the observation. At somewhat

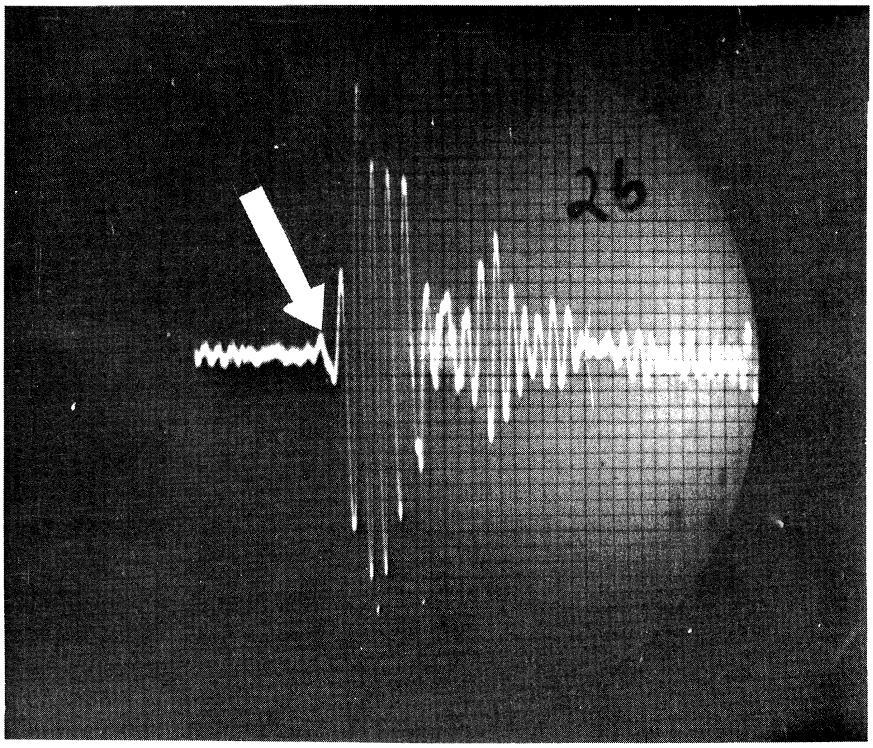

Fig. 33. Photograph of oscilloscope screen showing example of bottom transmitted early arrival (see arrow). Electrical pick-up at extreme left is not to be confused with the early arrival.

greater ranges there is evidence for an early arrival travelling with the approximate velocity of the compressional wave in concrete in addition to the one described. P.N.S. O'Brien[6] has with a similar experimental arrangement employing exponentional pulse forms obtained quantitative data regarding the amplitudes of the so-called "head" wave. He worked with a water-over-concrete model and observed close to the interface direct to compressional and direct to shear wave amplitude ratios of the order of 1:100 and 1:10 respectively. One may deduce from these ratios a compressional to shear wave amplitude ratio of the order of 1:10. Since in our experiments the shear wave signal (if it is shear) is very low in amplitude, one might expect that the compressional wave signal is down in the background noise. It is hoped that the questions raised here can be resolved eventually. Further effort in this problem of bottom-propagated energy is planned.

A number of runs employing a 10 kcps one-millisecond signal were made. These have proved difficult to interpret for the reason that a "spool effect" was obtained on the transmitted pulse. This phenomenon makes it difficult to identify reflected pulses and obviates amplitude measurements.

3.2.4. Study of Bottom Characteristics

It is well recognized and has been further emphasized in the theoretical treatment of the model program that in shallow water sound propagation, especially at frequencies below 5 to 10 kcps, one must evaluate the degree to which the elastic properties of the bottom influence the sound field. These properties influence such questions as the amount of energy lost in the bottom, the energy re-radiated by the bottom, the velocities with which the energy is propagated in the bottom, and the critical angles of reflection at the bottom for water-propagated waves. For these reasons several independent measurements were made to determine the values of the pertinent elastic constants of the concrete bottom of the tanks employed in the experiments.

The concrete agglomerate contains pebbles ranging in size from that just visible to the naked eye up to those with a cross-section of about one inch. The density, as determined by weighing a large representative bottom sample, is 2.3 grams/cc. The thickness of the concrete varies between five and seven inches. It has been laid in sections each about 30 feet square. The sections are separated by one-half inch of an expansion joint material composed of asphalt-impregnated paper. The bottom of the first tank used had been further broken in many places; many cracks are clearly visible. The bottom of the second tank exhibits no such cracks.

The methods that have been used in an attempt to determine the elastic properties of the bottom are briefly described below.

a. Dynamic method - Prismatic bars of concrete sawed from the bottom were vibrated in various longitudinal and torsional modes using a concrete testing apparatus in the Michigan State Highway Department Laboratory. No information was gained due primarily to the difficulty in exciting suitable modes in the bars of the small dimensions available.

b. Static compression method - A prismatic bar of concrete was compressed and the resultant strain measured. No conclusive information was obtained since strains were localized by the inhomogeneities and yielded an excessive spread in the data.

c. Impulse method - A test bar of the concrete was sent to the Shell Exploration and Development Company for a determination of the velocities of propagation and attenuation of acoustical pulses. This was done in response to an offer by Dr. A. Ginzbarg of that company to make the measurements with an apparatus which they use for similar determinations. The method consists of coring the concrete sample, measuring transit times and pulse amplitudes in the core, and then cutting the sample into two unequal parts and repeating the experiments.

These pieces are then saturated with water after being evacuated, and the measurements repeated. The method gives three points on plots of time versus length and amplitude versus length for both dry and wet samples. The frequency of observed pulses was approximately 10 - 15 kcps.

The velocity data from both dry and wet samples gave consistent values from sample to sample. The values of velocity as obtained from graphs of travel time versus sample length are shown below.

	Dry	Wet
c_c (compressional velocity)	15,350 ft/sec	16,250 ft/sec
c_s (shear velocity	9,160 ft/sec	8,960 ft/sec

Shear wave attenuation was also measured by observing the difference in amplitude between once and twice reflected shear pulses. Corrections were made on the basis that both attenuation and reflection coefficients affect the observed amplitude. The actual value for the shear attenuation in the wet samples seemed to be about 1/3 db/cm (within a factor of two). Such a value is close to the upper limit of attenuation and, in general, one must expect that the attenuation is actually somewhat less.

d. Reflected pulse method - This technique has been adequately described above in the discussion concerning the one-millisecond pulse experiments. As was explained there a discrepancy exists between the values obtained in this manner and those obtained by method c.

e. Early arrival method - Now that definite observation of early arrivals (see "One-millisecond pulse experiments" above) has been made, it should be possible with refined experiments to get a reliable check on the velocities obtained by the reflected pulse method previously described. In the second tank one can work within a single concrete block with no cracks in the bottom over the working range.

IV. SUMMARY AND CONCLUSIONS

The results of the experimental work may be classified in two ways. One set of results provides information about the acoustic characteristics of the water tanks. The other deals with the more general problem, namely the characteristics of the propagation of sound in shallow water.

4.1.1. The Acoustic Characteristics of the Tanks

The Bottom - Various standard experimental techniques and one rather unique one have been employed to determine values for the physical constants of the concrete bottom of the tanks. These have been described in Section 3.2.4. From the experiments two sets of values for the velocities of propagation of the compressional and shear waves associated with the concrete have been obtained. Although the two sets of values differ in a ratio of 4:3, both lie in a range of velocities which are reasonable for concrete.

Remembering the difficulty of ascertaining the true values for the physical constants of the concrete, a reasonable similarity has been found between the measured and calculated sound fields over the ranges employed in the tanks. It has been shown that the assumption of a perfectly rigid bottom is a fair approximation to the existing situation. In addition the calculation including the effect of a compressional wave in the bottom (fluid bottom) bears unmistakeable resemblance to the

measured sound field. The basic reason for the similarity between the rigid and fluid bottom calculations lies in the fact that in the situation for which calculations were made, four normal modes are propagating in either case.

It appears that agreement between the calculation and the measured field will be improved by more accurate determination of the physical constants.

In the short pulse experiments where the amplitude-range dependence of the source images was measured, it was found that over the path lengths and number of associated bottom reflections considered, little attenuation was apparent. This implies low energy loss per bottom reflection. It is necessary to postulate only a slight loss per reflection to account for considerable attenuation of the normal modes at long ranges.

No evidence has been found to lead the authors to believe that the bottom cannot be considered a semi-infinite half-space at least at the frequencies of interest. In the Appendix to Section 3.1 a calculation indicates that the above conclusion is probably correct. Experimentally no reflected pulses attributable to reflections from the interface between the bottom of the concrete and the ground or from the ground below have been observed.

4.1.2. The Effect of Other Factors

In the course of the experiments several factors, other than the bottom and its effect upon the acoustic characteristics of the tanks, were investigated. For example, the measured sensitivity of the sound field to variations in water depth, receiver depth, and frequency is shown in Fig. 34a, b, c and the ΔH effect, Δd effect and Δf effect, respectively. The plots of pulse data were selected to demonstrate the

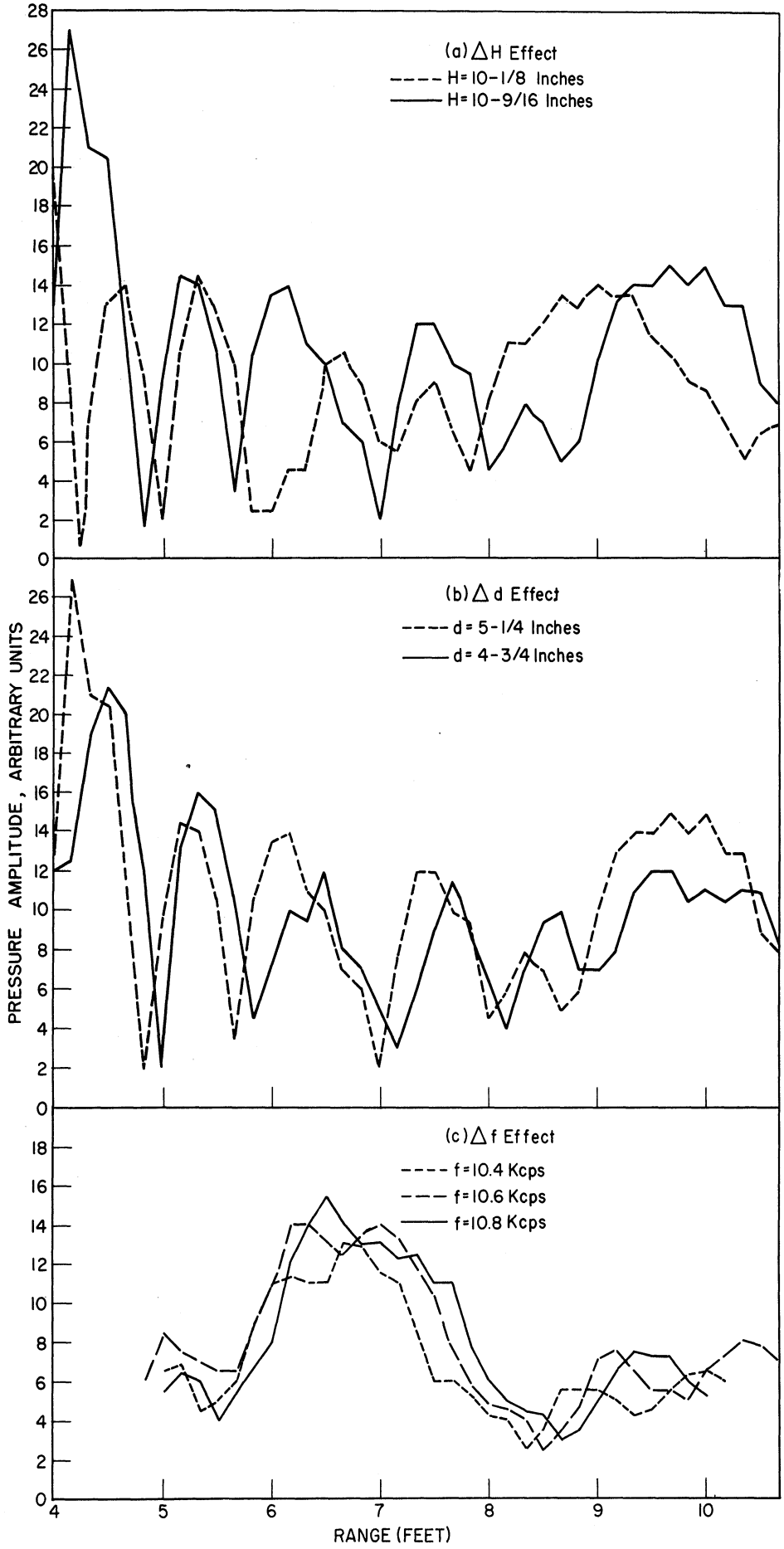

Fig. 34a, b, c. Effect of slight variations in water depth, receiver depth, and frequency.

order of magnitude of the shift in the sound field with small changes in individual variables. They serve merely to point out the care with which the parameters must be controlled in order to obtain repeatable results.

The degree to which the bottom approximates a level surface has been examined along the range under the trolley track. The steepest slope found amounted to 0.004 ft/ft over a 10 ft range. This is a slope of 14 minutes. Over a 40 ft range interval the slope was more like 0.0015 ft/ft or 5 minutes. Variations of depth and bottom slope of this order of magnitude are not believed significant over the range and with the water depths employed in these experiments.

Water temperature has been measured each day near the surface, at mid-depth and near the bottom. The total spread between the top and bottom is generally less than 2°C. This has been considered a minor effect insofar as the gradient is concerned. To determine the sound velocity for use in computations an average temperature, which is near the mid-depth temperature, is used. The velocity of sound at the average temperature is taken from British Admiralty Tables of the velocity of sound in fresh water.(7)

The problem of wall reflections has been examined. It seems clear that when conditions are such that more than three or four modes are propagating, wall reflections must begin to contribute significantly to the observed signal. For example this occurs with deeper water or higher frequency, or both. By shortening the pulse it is possible to observe in a region wherein the wall reflections do not arrive in time to influence the measurement. One approach to the solution of the problem of working with higher numbers of propagating modes is to change the scale factor. This can be done by lowering the water depth and raising the frequency to the limit imposed by the fact that the bottom is not perfectly level. To observe the sound fields at ranges longer than 40 or 50 λ such a change is necessary anyway.

It does not appear that wall reflections offer a suitable explanation for the high amplitude interference signal superimposed on the modal field at range intervals of approximately $\lambda/2$. The possibility that the interference is the result of re-radiated bottom-propagated energy has been posed. It is considered more likely that the normal modes of order number higher than four (presumed heretofore to be highly damped) are the source of this phenomenon. Particular attention is being given the attenuation of these modes in order to determine their contribution to the sound field.

That the departures of the calculations from the measurements are probably related to the bottom constants is further emphasized by the results of experiments utilizing different bottom types. One set of measurements was taken with a fiber glass bottom. Asphalt covered fiber glass 7/8" thick was placed over the concrete along the range. The sound field was measured with $H/2 = h = d = \lambda$. The periodic nature of the pressure amplitude vs range plot indicated a field with two propagating modes. Assuming the water layer was bounded by pressure release surfaces, a calculation of the spacing of the modal interference peaks was made. The calculated spacing was just three per cent different than the measured spacing. The fact that good agreement was obtained serves to indicate that the assumption of a pressure release bottom was correct and that no spurious effects were encountered from the bottom or from wall reflections. It may be inferred then that effort must be placed on the problem of arriving at consistent and reliable values for the velocities and energies of the waves propagated in the concrete bottom.

Another experiment was carried out utilizing a bottom of sintered clay blocks laid over the concrete. The effect upon the sound field was that which would be anticipated with a bottom which is "lossy". In one millisecond pulse runs the amplitudes of the top-and bottom-reflected pulses were observed to fall rapidly with range.

In summarizing the acoustic properties of the tanks it can be stated that they offer a definite promise of value in their employment as shallow water models. The degree of versatility of the model, particularly in investigating the sound propagation mechanisms acting in the near and intermediate fields, has been suggested in this report and is reviewed below in Section 4.1.3. It is believed that work in progress will solve the problem of the inconsistency in the values of the elastic constants of the concrete bottom. Once this has been done the more serious application of the model to shallow water sound propagation problems will begin. The restrictions imposed by wall reflections and/or concrete-propagated energy are not believed to be serious. The extent to which ranges can be lengthened probably in the final analysis will be determined by the bottom roughness.

4.1.3. The Propagation of Sound in Shallow Water

In the investigation of the acoustic properties of the tanks and the probable value of the tanks as models, several interesting factors related to propagation have been explored. The following summary of these factors serves to exemplify the different types of problems to which the model can be applied.

First the convenience of the model for making rapid checks on theoretical results and on certain calculations is evident. Within the capabilities of the model one is able to set up an experiment and very often in the period of a day or two have a set of pertinent data. Such a procedure enables both the theoretical and experimental phases of the program to procede with a minimum of extraneous difficulty. At the present time this procedure is being utilized in the investigation of the role of presumably damped modes and branch-line integral contributions in the near and intermediate sound field.

It has been shown that the model offers a good facility for the determination of the frequencies at which the normal modes cease to be highly damped in a prescribed situation. With little additional complication of the experiment one can also expect to observe changes in the energy in the sound field associated with mode cut-ons. This type of experiment includes the capability for the examination of the excitation function as a function of frequency. Thus both frequency and amplitude studies of the Airy phase can be made.

While no effort has been expended in this type of investigation, attention has been given to the possibility of exploring certain other modal mechanisms which are of considerable interest. These are the examination by means of pulses of the build-up of modes at longer ranges and the examination of the decay or the conversion of higher modes to lower modes due to scattering using a c-w signal at long range. Scattering caused by bottom irregularities (using larger scale factors) and by a roughened water surface are possible mechanisms to employ in the latter problem. An investigation of the effect of the shear wave attenuating in the bottom would also be of interest. In the former problem it can be shown that as the path lengths of the various source image signals approach that of the direct signal at long ranges, the pulses will merge in time to form modes. As these modes are formed one should be able to observe their group velocities and amplitudes.

Some effects of varying pulse length upon the form of the received signal have been observed. Qualitatively these observations are in agreement with those computed using the approximate normal mode method and the image series summation method. It is believed that a rigorous experimental and theoretical program concerned with these c-w pulses could possibly result in the development of practical techniques applicable to the investigation of propagation mechanisms in the ocean.

In the matter of determination of reflection coefficients of the bottom it is proposed that the technique employed in Section 3.2.3 of this report be considered as a practical shallow water technique. Here c-w pulses were used, and the pressure amplitude-range dependence of the various orders of the received pulses was observed. The critical angles for cut-off of the compressional and shear bottom propagated waves (and so the velocities) were determined by observing peaks in the amplitude curves. The multiple reflections provide a convenient means of measuring mode attenuation. Simultaneous measurements at a few select frequencies could reveal a great deal regarding the bottom characteristics and transmission loss.

Two preliminary experiments which were performed employing bottom types different from the concrete bottom have been described above. These represent the attempts made thus far to change the bottom material. The possibility of introducing various bottom materials and configurations in the model gives rise to a number of feasible experiments. One of the advantages offered by the model in this type of experiment is the possibility of extending the pressure amplitude measurements into the bottom materials. Thus direct measurements of velocity, amplitude, and attenuation in the bottom materials could be made.

In summary it is believed that the model discussed in this report can be employed to investigate some of the probable mechanisms which may account for the attenuation of the sound propagating in shallow water. The more probable mechanisms include (1) depth variations; (2) attenuations produced by the non-plane upper surface; (3) attenuations due to scattering at the lower surface; and (4) attenuations produced by dissipation in the bottom.

(Continued from page 47)

BIBLIOGRAPHY

5. Marvin S. Weinstein, J. Acoust. Soc. Am., 24, 284 (1952).

6. Peter N.S. O'Brien, "Model Seismology - The Critical Refraction of Elastic Waves", Geophysics 20, 227 (April 1955).

7. Mathews, D.J., "Tables of the Velocity of Sound in Pure Water and Sea Water for Use in Echo-Sounding and Sound Ranging" 2nd Ed., Hydrographic Dept. British Admiralty, 1939 p. 282.

UNCLASSIFIED

Distribution list for Technical Reports
University of Michigan
Contract N6onr 232(21), NR 385-203

Office of Naval Research
Acoustics Branch (Code 411)
Washington 25, D.C. (2 copies)

Office of Naval Research
Undersea Warfare Branch (Code 466)
Washington 25, D.C. (1 copy)

Director
Naval Research Laboratory
Technical Information Officer
Washington 25, D.C. (6 copies)

Commanding Officer
Office of Naval Research Branch Office
1030 E. Green Street
Pasadena 1, Calif. (1 copy)

Commanding Officer
Office of Naval Research Branch Office
10th Floor
The John Crerar Library Bldg.
86 E Randolph Street
Chicago 1, Ill. (1 copy)

Commanding Officer
Office of Naval Research Branch Office
346 Broadway
New York 13, N.Y. (1 copy)

Commanding Officer
Office of Naval Research
Navy No. 100, Fleet Post Office
New York, New York (1 copy)

Office of Technical Services
Department of Commerce
Washington, D.C. (1 copy)

Armed Services Tech. Infor. Agency
Document Service Center
Knott Building
Dayton 2, Ohio (5 copies)

Director
Naval Ordnance Laboratory
White Oak, Md.
Attn: Sound Division (1 copy)

Commanding Officer and Director
U.S.N. Underwater Sound Lab.
New London, Conn. (1 copy)

Commanding Officer and Director
U.S.N. Electronics Laboratory
San Diego 52, Calif. (1 copy)

Commander
Naval Air Development Center
Johnsville, Pa. (1 copy)

Chief,
Bureau of Ships (Code 847)
Navy Department
Washington 25, D.C. (1 copy)

Superintendent,
U.S. Navy Postgraduate School
Physics Department
Monterey, Calif.
Attn: Prof. L.E. Kinsler (1 copy)

Harvard University
Acoustics Laboratory
Division of Applied Science
Cambridge 38, Mass. (1 copy)

Catholic University of America
Department of Physics
Washington 17, D.C.
Attn: Dr. K. Herzfeld (1 copy)

Brown University
Department of Physics
Providence 12, Rhode Island
Attn: Prof. A.O. Williams (1 copy)

Mass. Institute of Technology
Acoustics Laboratory
Cambridge 39, Mass. (1 copy)

Director,
Marine Physical Laboratory
University of California
U.S. Navy Electronics Laboratory
San Diego 52, California (1 copy)

Hudson Laboratories
Columbia University
145 Palisades Street
Dobbs Ferry, N.Y. (1 copy)

Distribution List (Continued)

Lamont Geological Observatory
Columbia University
Torre Cliffs
Palisades, N.Y. (1 copy)

Woods Hole Oceanographic Institution
Woods Hole, Massachusetts (1 copy)
Attn: J.B. Hersey

U.S. Undersea Warfare Committee
Navy Department
Washington 25, D.C.